Medicinal Chemistry Research (2021) 30:1614–1634
https://doi.org/10.1007/s00044-021-02760-3

MEDICINAL CHEMISTRY RESEARCH

ORIGINAL RESEARCH

# Design and synthesis of new pyrazolylbenzimidazoles as sphingosine kinase-1 inhibitors

Shadia A. Galal[1] · Mohamed A. Omar[1] · Sarah H. M. Khairat[1] · Fatma A. F. Ragab[2] · Sonam Roy[3] · Ahmad Abu Turab Naqvi[3] · Md. Imtaiyaz Hassan[3] · Hoda I. El Diwani[1]

Received: 18 March 2021 / Accepted: 9 June 2021 / Published online: 29 June 2021


## Abstract

Sphingosine-1 kinase (SphK1) is one of the important enzymes of phospholipids and its inhibition is one of the therapeutic strategies for different diseases. SphK1 over expression is observed in different types of cancer indicating its important role in tumor growth. In search of effective SphK1 inhibitors, a new series of pyrazolylbenzimidazoles was synthesized and evaluated as sphingosine kinase-1 (SphK1) inhibitors. In order to evaluate the binding affinities of all the synthesized compounds, all compounds were subjected to docking analysis and fluorescence quenching. The results indicated that there is a consistency between the docking and the fluorescence quenching results, which revealed that compounds **47** and **48** exhibited significant decrease in the fluorescence intensity of SphK1 as well as they formed stable protein–ligand complexes. In addition, enzyme inhibition assay was performed which showed effective inhibitory potential toward SphK1. Moreover, $IC_{50}$ values displayed that compounds **47** and **48** were the most promising compounds. In addition, antiproliferation study for all the synthesized compounds was performed against NCI-60 cell line panel. The target compounds **47** and **48** demonstrated effective antitumor activity and growth inhibitory potential toward cancer cell lines. Most of these compounds fit well into the ATP-binding site of SphK1 and form significant hydrogen-bonding interactions with catalytically relevant residues as predicted by molecular docking. In this article, insight has been given for the importance of pyrazolylbenzimidazoles as SphK1 inhibitors and the perspectives that they hold for future research.

## Graphical Abstract

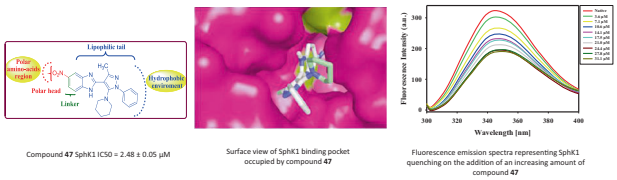


**Keywords** Benzimidazole · Pyrazole · Sphingosine kinase-1 (SphK1) inhibitors · Antitumor activity · Molecular-docking study

**Supplementary information** The online version contains supplementary material available at https://doi.org/10.1007/s00044-021-02760-3.

✉ Shadia A. Galal
sh12galal@hotmail.com

✉ Fatma A. F. Ragab
fatmarag@hotmail.com

[1] Division of Pharmaceutical and Drug Industries Research, Department of Chemistry of Natural and Microbial Products, National Research Centre, El-Buhouth St., Dokki, P. O. Box 12622, Cairo, Egypt

[2] Faculty of Pharmacy, Department of Pharmaceutical Chemistry, Cairo University, Cairo, Egypt

[3] Centre for Interdisciplinary Research in Basic Sciences, Jamia Millia Islamia, Jamia Nagar, New Delhi 110025, India

## Introduction

Sphingolipid is a kind of phospholipid, which is a major component of all cell membranes and can form lipid bilayers that maintain the fluidity of membranes [1]. Ceramide (Cer), sphingosine (Sph), and sphingosine-1 phosphate (S1P) are metabolites of sphingomylein, which play an important role in different diseases such as cancer [2, 3], fibrosis [4], and Alzheimer's disease [5]. The balance between the sphingolipid metabolites, which act in two opposite ways, is crucial in the determination of the cell fate [6, 7]. Cer and Sph [8, 9] are a proapoptotic molecule to mediate the cell cycle and induce apoptosis, while S1P promotes cell proliferation and acts as a "pro-survival" molecule [10, 11]. Phosphorylation of the proapoptotic D-erythro-Sph to the promitogenic S1P is catalyzed by Sphingosine kinases (SphK). The two SphK isoforms (SphK1 and SphK2) are known to catalyze this transformation and regulate the sphingolipid metabolism. In particular, SphK1 is more closely linked in many diseases such as cancer, rheumatoid arthritis, diabetes, asthma, and pulmonary fibrosis [12–14]. Studies have shown that over expression of SphK1 is observed in many tumor tissues and regulating tumorigenesis, angiogenesis, and chemotherapy resistance, which play an important role in cancer progression [15–20]. Hence, inhibition of SphK1 is considered a new therapeutic strategy in the treatment of metastatic cancer and other diseases [21, 22].

SphK inhibitors can be classified into SphK1-selective inhibitors and SphK1/SphK2-dual inhibitors. Many compounds were reported to be a potent selective SphK1 inhibitors, e.g., *N*,*N*-dimethylsphingosine **1** [23] and compound (FTY720) **2** [24, 25] (Fig. 1). Moreover, compound (CS0777) **3** [24, 26] and compound (PF-543) **5** [27, 28] are examples of an orally active SphK1 and (SKI-II-Asp) **4** [24] (Fig. 1). On the other hand, compounds **6** (SKI-III) [29–32] and **7** (Amgen 23) [33] were reported as SphK1/SphK2-dual inhibitors (Fig. 1).

Compounds **8** (SKI-I), **9** (SKI-I-Asp), and **10** (SKI-178), which possess pyrazole ring in their structures, exhibited potent inhibitory effect on SphK1 (Fig. 2) [24, 34]. Recently, large numbers of 2-substituted benzimidazoles were discovered to have potent inhibitory effect on SphK1 [34–36]. The benzimidazoles **11** and **12** (Fig. 2) were reported as SphK1 inhibitors [35, 36]. The benzimidazole moiety is well known to interact with kinases by multiple binding modes [35, 37–39].

From the ongoing information, our group has reported different ways for the synthesis of benzimidazoles [40–49] targeting different kinases. In this study, our aim is to design and synthesize Sph kinase-1 inhibitors by the combination of both pharmacophoric moieties benzimidazoles and pyrazoles.

The evolution of SphK1 and SphK2 inhibitors has been recently reported [50, 51]. Many SphK inhibitors were designed to have a polar head group and a lipophilic tail region. Studying all structural variations in the Sph-based SphKIs and their resulting biological effects in the earlier work, several points were taken into consideration to improve the potency of the new target compounds possessing both pharmacophoric moieties, benzimidazole and pyrazole: (1) In the lipophilic region: increasing lipophilicity by introducing saturated heterocycles to the pyrazole ring as $R_2$ = morpholinyl, piperidinyl, and pyrrolidinyl in the lipophilic tail as well as the introduction of a phenyl ring will enhance the lipophilicity and the bioavailability by producing a better drug-like profile. (2) In the polar head: replacing the hydroxyl group to prevent its phosphorylation by other polar groups seems to be vital in the design of new Sph-based SKIs. Modification of the polar head to possess the following groups: $R_1 = NO_2$, $COOH$, was planned so that the nitro group and the carboxylic group will be the polar heads (Fig. 3).

## Results and discussion

### Chemistry

The present study aimed to synthesize new benzimidazole candidates as Sph kinase-1 inhibitors (Fig. 3) and it was guided by molecular-docking study assessing their binding energies taking into consideration that polar substitution of the benzimidazole ring at 5 position was essential for activity. The target pyrazolylbenzimidazoles derivatives were synthesized through two main schemes. The first part of this synthesis was demonstrated in Scheme 1, which deals with the preparation of pyrazole derivatives via three steps starting by the synthesis of 3-methyl-1-phenyl-pyrazol-5-one **13** by the reaction of phenyl hydrazine with ethyl acetoacetate in the presence of glacial acetic acid and ethanol according to the procedure described by Prajuli et al. [52]. The Vilsmeier–Haack reaction of the previous step afforded 5-chloro-3-methyl-1-phenylpyrazole-4-carboxaldehyde **14**, which followed by introduction of nucleophiles i.e., secondary amines or phenol derivatives to give compounds **15–21** (Scheme 1) [52–55]. The second part of this synthesis was the coupling of pyrazole-4-carboxaldehydes **15–21** with 1,2-benzendiamine **22**, 3,4-diaminobenzoic acid **23**, 4-methylbenzene-1,2-diamine **24**, or 4-nitrobenzene-1,2-diamine **25** to afford different derivatives **26–48** (Scheme 2). Based on the predicted binding affinities and interactions, compounds **47** and **48** were selected as top-scoring compounds and modification of the polar head to possess the $NO_2$, group was planned. Unfortunately, the low yield and poor solubility caused no synthesis of other derivatives of nitro-analogs.

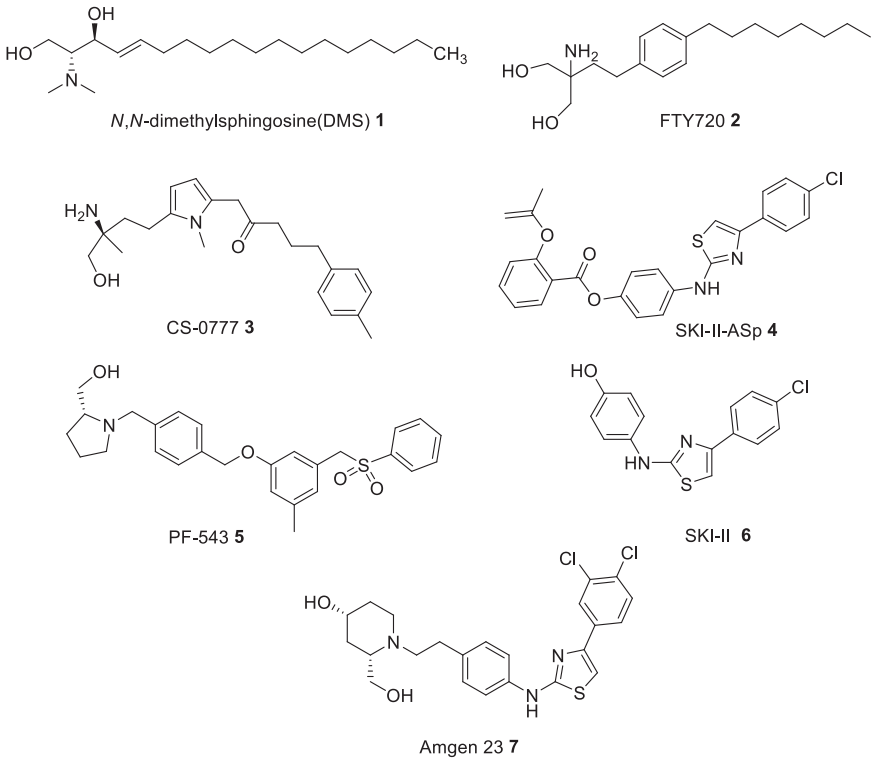


**Fig. 1** Examples of sphingosine kinasel inhibitors

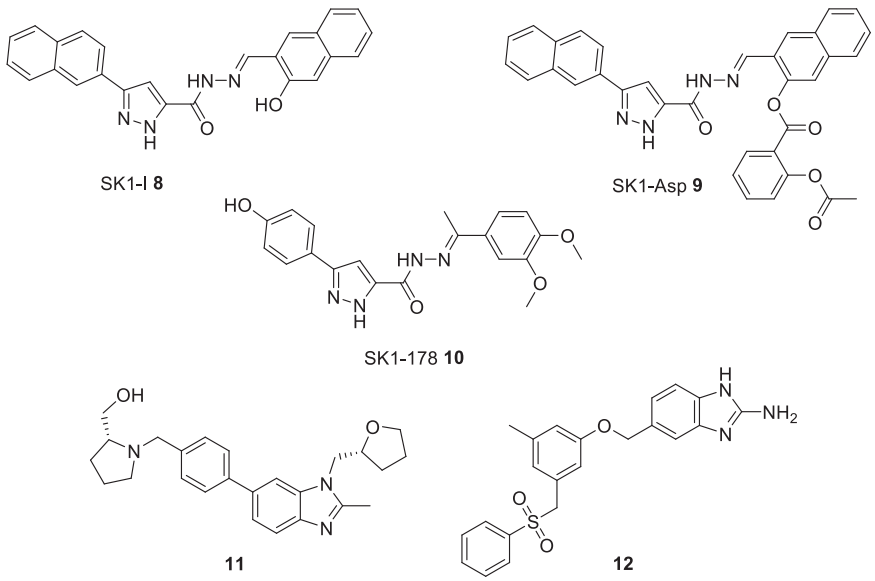


**Fig. 2** Examples of benzimidazoles and pyrazole derivatives as SphK1 inhibitors

## Fluorescence binding studies

Fluorescence binding studies were performed for evaluating the binding affinity of all the synthesized compounds **26–48** with SphK1. The gradual loss in the fluorescence intensity upon addition of the selected compounds, **47** and **48** (Figs. 4A, B), was observed for SphK1, which points toward the formation of a stable protein–ligand complex. The rest of the compounds did not show any quenching and some of them even perturbed the structure of SphK1 since major red shift and increase in the fluorescence intensity was observed when added to protein samples in increasing concentrations (Fig. S24–27). The Stern–Volmer plot (Fig. 4C, D) was used to analyze the quenching data to determine the binding affinity ($K_a$) for each compound. The number of binding sites per SphK1 molecule ($n$) for these compounds was also determined

from the same plot. Compounds **47** and **48** showed binding in the $10^4$ and $10^3$ micromolar, respectively (Table 1). Thus, hits obtained from the binding studies showed moderate binding with SphK1 and were further tested for inhibitory activity against SphK1.

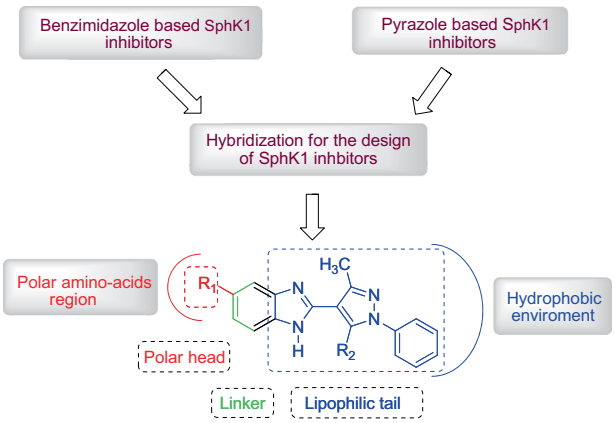


**Fig. 3** Rational design of new 5-substituted 2-pyrazolylbenzimidazoles as sphingosine kinase-1 inhibitors

## Enzyme inhibition assay

Enzyme inhibition potential of compounds **26–48** toward SphK1 was evaluated by malachite green ATPase inhibition assays. During the initial screening, the maximum concentration of all compounds (100 µM) was used (Table S2), which revealed that most of the studied compounds inhibited SphK1 activity effectively (Table 2). Further, the $IC_{50}$ values of the synthesized compounds that showed good binding affinity toward the SphK1 were evaluated and found to be in the micromolar range (Table 3). The kinase activity of SphK1 is measured in terms of picomolar concentration of phosphate released in the reaction mixture, which is represented in Fig. 5A, B. The absorbance value of the malachite-inorganic phosphate green complex so formed at 620 nm is converted with the help of phosphate standard curve as described [56–63]. The loss in the SphK1 activity followed an inverse relationship between percentage inhibition and an increasing concentration of selected compounds as shown in Fig. 5C, D, which was used for the calculation of $IC_{50}$ values (Table 3). The compound **47** efficiently inhibited SphK1 kinase activity with lower $IC_{50}$

**Scheme 1** Synthetic route of pyrazole-4-carboxylate derivatives 15–21. Reagents and conditions: (i) $Na_2S_2O_5$, ethanol. Reagents and conditions: (i) EtOH, glacial acetic acid, reflux, 8 h; (ii) phosphorus oxychloride, DMF, reflux 2 h; (iii) morpholine, piperidine or 1-methyl piperazine, $K_2CO_3$ DMF, reflux 3 h; (iv) pyrrolidine, $K_2CO_3$ DMF, reflux 3 h; (v) phenol, 2-hydroxypyridine or 2,5-dimethylphenol, $K_2CO_3$ DMF, reflux 3 h

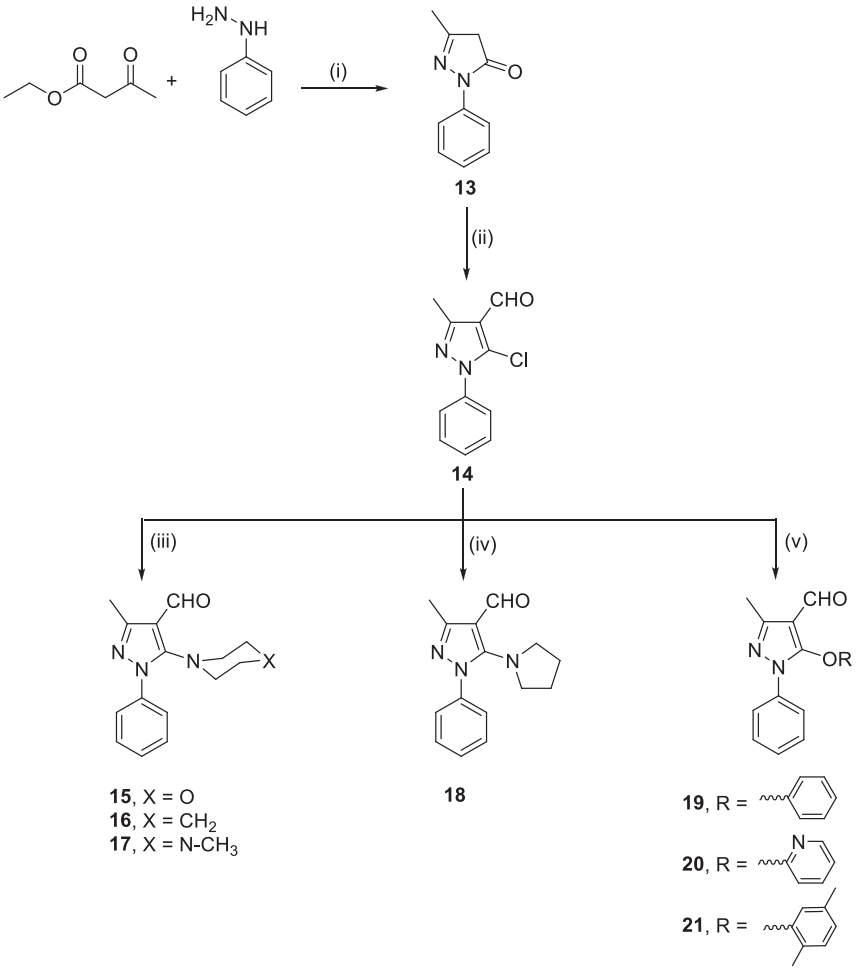

**Scheme 2** Synthetic route from pyrazole **15–21** to pyrazolylbenzimidazole derivatives **26–48**

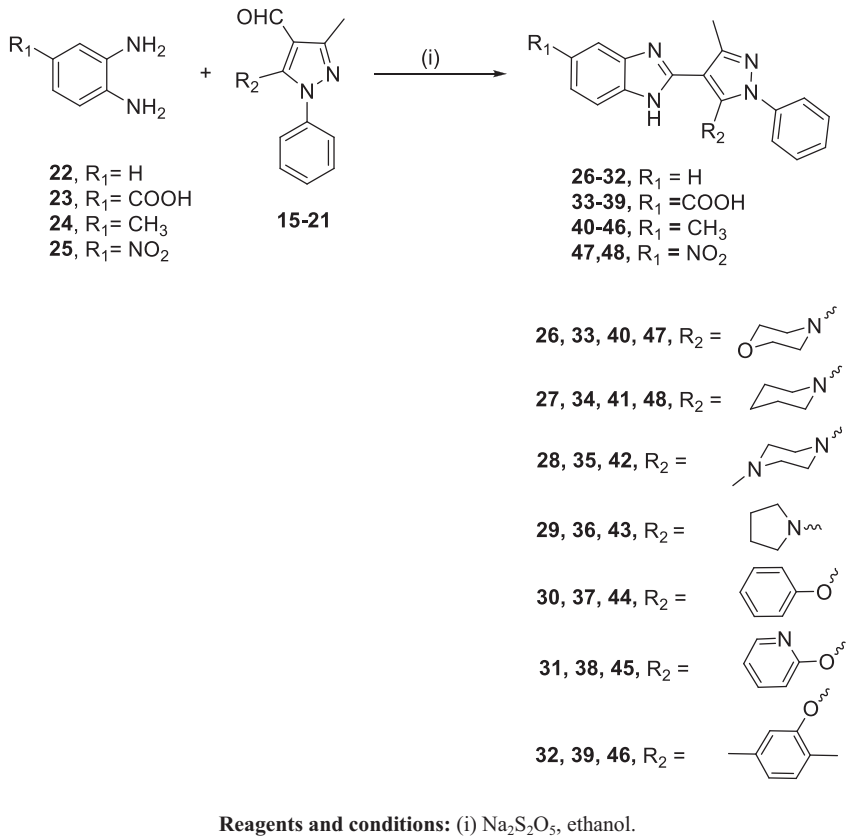


**Reagents and conditions:** (i) $Na_2S_2O_5$, ethanol.

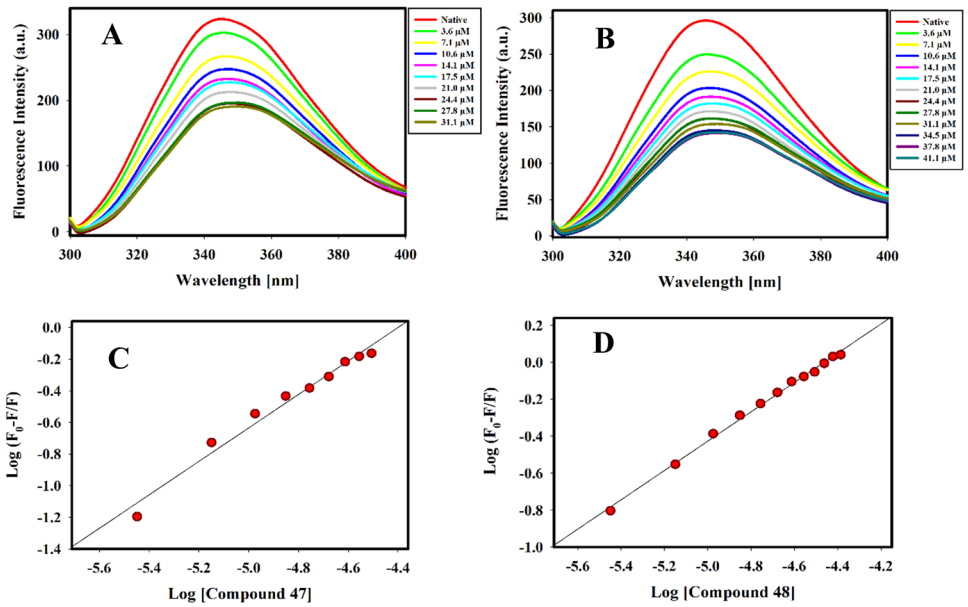


**Fig. 4** Binding studies of selected synthesized compounds with SphK1. Fluorescence emission spectra representing SphK1 quenching on the addition of an increasing amount of **A** compound **47** (0–31.1 µM), **B** compound **48** (0–41.1 µM), SphK1 was excited at 280 nm and emission spectra were recorded in the range of 300–400 nm. Modified Stern–Volmer plot was used to analyze the quenching data and to estimate the binding constant ($K_a$) for **C** compound **47**, **D** compound **48**

(2.48 ± 0.05 µM). Compound **48** (Fig. 6D) inhibited SphK1 activity with a slightly higher $IC_{50}$ (4.02 ± 0.16 µM). The $IC_{50}$ values of compounds **47** and **48** on comparison with some of the reported synthetic SphK1 inhibitors, suggested that, compounds **47** and **48** are less effective than SKI-178 (0.1–1.8 µM), PF-543 (3.6 nm), and Amgen 82 (20 nm) in inhibiting SphK1 activity while more potent inhibitor than DHS (5 µM), SKI (10 µM), SK-II (16 µM), and FTY720 (5–12.5 µM) [64, 65]. The enzyme inhibition results overall propose that compounds **47** and **48** act as promising leads for development of selective inhibitors of SphK1 with high potency.

**Table 1** The binding affinity constants and number of binding sites as determined from the molecular docking and fluorescence binding experiments

| Compound no. | Predicted affinity ΔG[a] (kcal/mol) | [b]Binding affinity constant ($K_a$), $M^{-1}$ | [b]Number of binding sites ($n$) |
|---|---|---|---|
| **47** | −8.0 | $4.52 \times 10^4$ | 1.1 |
| **48** | −7.9 | $3.46 \times 10^3$ | 0.8 |

[a]Binding parameters of the synthesized compounds with SphK1 evaluated through molecular docking

[b]Binding parameters of the synthesized compounds with SphK1 evaluated through fluorescence binding studies

**Table 2** Kinase assay: % of inhibition of compounds **26–48** toward SphK1 enzyme

| Compound no. | % of inhibition | Compound no. | % of inhibition |
|---|---|---|---|
| **26** | 61.43% | **38** | 95.01% |
| **27** | 89.58% | **39** | 94.28% |
| **28** | 92.66% | **40** | 96.18% |
| **29** | 70.38% | **41** | 93.25% |
| **30** | 96.04 | **42** | 92.37% |
| **31** | 88.70% | **43** | 75.51% |
| **32** | 95.30% | **44** | 70.52% |
| **33** | 64.95% | **45** | 95.89% |
| **34** | 87.53% | **46** | 80.20% |
| **35** | 93.40% | **47** | 98.82% |
| **36** | 78.98% | **48** | 96.48% |
| **37** | 93.69% | | |

**Table 3** $IC_{50}$ values of the selected compounds for SphK1 inhibition calculated from the ATPase inhibition assay

| Compound no. | $LogIC_{50}$ (μM) | $IC_{50}$ (μM) |
|---|---|---|
| **47** | 0.39 ± 0.01 | 2.48 ± 0.05 |
| **48** | 0.60 ± 0.02 | 4.02 ± 0.16 |

## Anticancer activity against NCI-60 cell line panel

Most of the synthesized compounds were screened for their in vitro antitumor activity by the Developmental Therapeutics Program of the National Cancer Institute (NCI) in the division of cancer treatment and diagnosis, NIH, Bethesda, Maryland, USA. This involves screening of the compounds at a single dose of 10 μM against a full NCI-60 cell panel including leukemia, lung, colon, brain, melanoma, ovary, kidney, prostate, and breast cancers [66]. From the obtained results in Table 4, it is obvious that each of the screened compounds has a different degree of selectively against 60 cell lines. K-562, MOLT-4, PRMI-8226, and SR from leukemia; SNB-75 from CNS Cancer; UACC-62 from melanoma; A498, ACHN, CAKI-1, and UO-31 from renal cancer; PC-3 from prostate cancer; and T-47D and MDA-MB-468 from breast cancer are the most sensitive cell lines to the tested compounds. The studied compounds showed a broad spectrum of anticancer activity against several NCI cell panels. At 10-μM concentration, compounds **47** and **48** showed potent inhibition against the leukemia and breast cancer cell lines (Table 4).

## Molecular docking

The molecular-docking study of the designed compounds with SphK1 was performed using the AutoDock vina tool [67]. Vina gives the predicted binding poses of the synthesized compounds **26–48** along with the binding affinities in kcal/mol. Based on the predicted binding affinities and interactions, compounds **47** and **48** were selected as top-scoring compounds. The predicted binding affinities of the selected compounds are given in (Table 5). On the basis of nonbonded interactions of compounds with the SphK1, compounds **47** and **48** showed comparatively better interactions. Figure 6 shows the 2D structure of compound **47** (Fig. 6A) along with its interactions with the PF-543 (binding affinity: 9.2 kcal/mol) binding site residues of SphK1 (Fig. 6B). Compound **47** forms hydrogen bonds with the Thr196 of the PF-543 binding pocket. 2D representation of protein–ligand interactions (Fig. 6C) shows compound **47** having π-interactions and van der Waals interaction with the surrounding residues including the Asp178, which is the substrate binding site. These interactions of compound **47** with SphK1 suggest a strong bonding. Surface view of the protein shows that compound **47** has strongly occupied the binding cavity of the protein (Fig. 6D). A similar pattern is observed for compound **48** where it forms a hydrogen bond with the Thr196 of the PF-543 inhibitor binding site; in addition, Ile174 and Leu302 are showing π–sigma interaction with the ligand (Fig. 7C). In addition to that, residues Val177, Leu268, Leu259, Ala274, and Leu319 are showing π–alkyl interactions with the ligand. Besides compounds **46** and **47**, a detailed interaction profile of all the synthesized compounds with SphK1 is given in Table 5. The docking figures for compounds **26–46** are given in the supplementary part (Figs. S28–48, respectively).

## Structure–activity relationship

Structure–activity relationships were illustrated from the previous results. Concerning the percent of inhibition of the

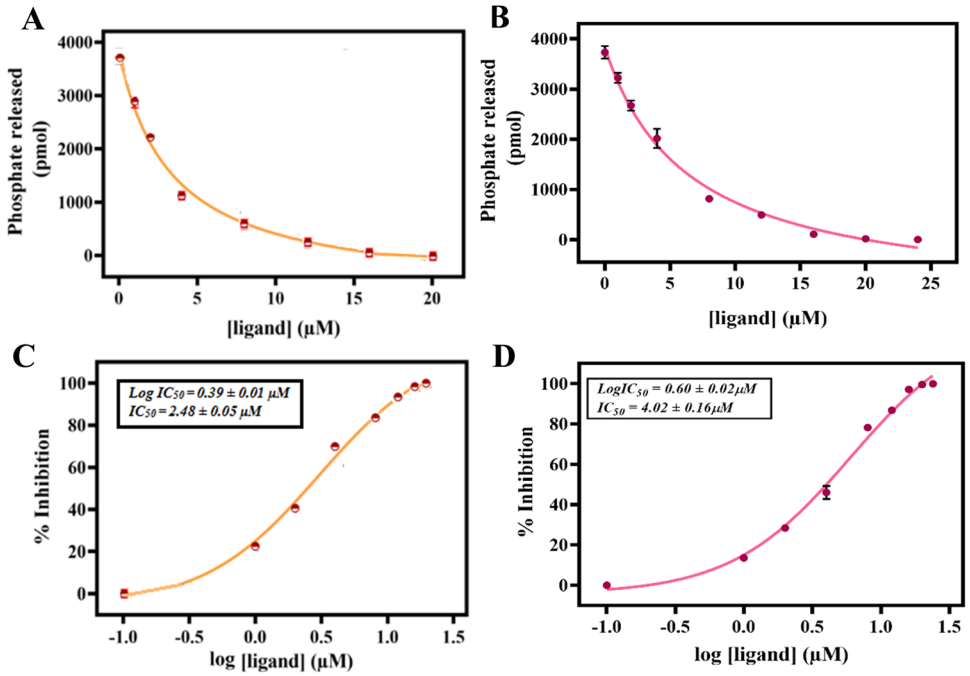


**Fig. 5** Inhibition of SphK1 ATPase activity by selected compounds. The amount of phosphate released from the hydrolysis of ATP was measured using the standard phosphate curve. Dose–response curve depicting the effect of increasing concentrations of **A** compound **47** (0–20 μM) on the ATPase activity of SphK1. Dose–response curve depicting the effect of increasing concentrations of **B** compound **48** (0–25 μM). Plots represent percent inhibition in ATPase activity of SphK1 as a function of increasing concentrations of **C** compound **47** and **D** for compound **48**. The $IC_{50}$ value was calculated by fitting the curve obtained from two independent experiments

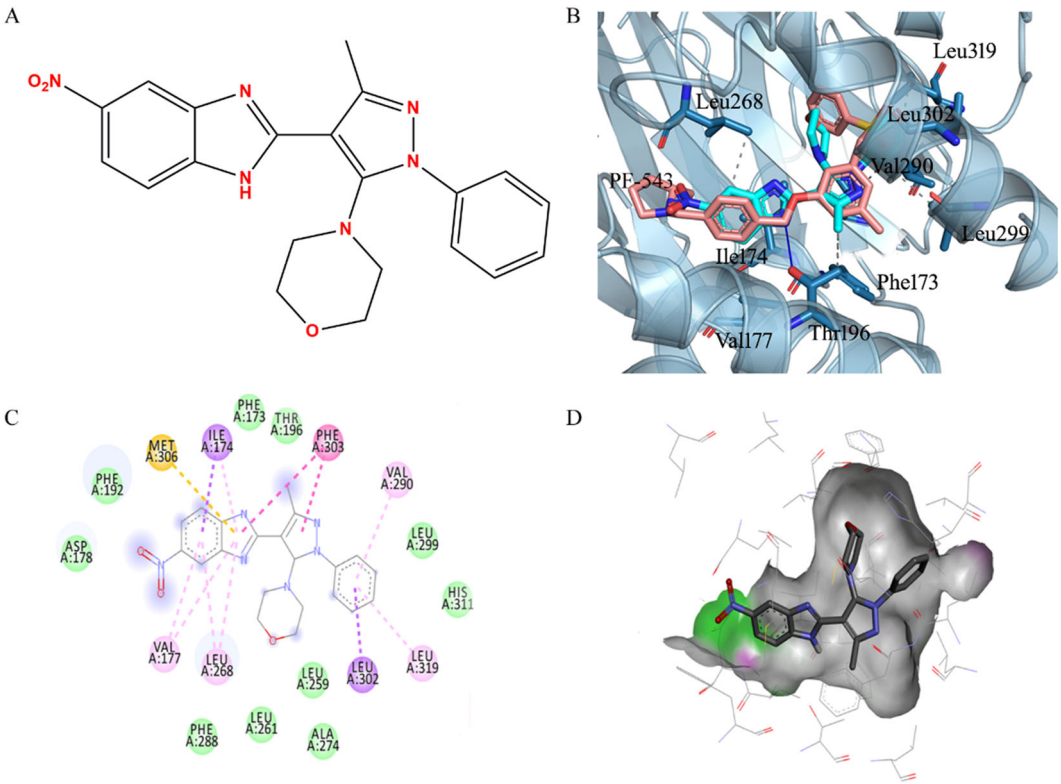


**Fig. 6** Compound **47** binding to SphK1 **A** chemical structure of compound **47**. **B** Graphical representation of PF-543 aligned with compound **47** interacting with binding site residues of SphK1. **C** 2D scheme of protein–ligand interactions. **D** Surface view of SphK1 binding pocket occupied by compound **47**

synthesized compounds toward SphK1, the following points can be explored. Most of the pyrazolylbenzimidazoles exert moderate to potent SphK1 inhibitory activity. Compounds **47** and **48** with $IC_{50} = 2.48 \pm 0.05$ and $4.02 \pm 0.16$, respectively, and percentage of inhibition 98.82% and 96.48%, respectively, are the most active compounds. It was observed the

importance of substituting the 5 position of benzimidazoles with nitro group. The correlation between the enzyme inhibition results, in vitro cytotoxic activity, and docking results was observed. This proves the importance of polar substituents at position 5 of the benzimidazole ring. Unfortunately, the low yield and poor solubility caused no synthesis of other derivatives of nitro-analogs. The unsubstituted benzimidazoles and 5-methylbenzimidazoles were synthesized as was predicted from the docking studies that they might possess good binding affinity but they were found to be the least active compounds. An increase in the inhibitory activity was observed by substitution at position 5 of the pyrazole moiety with *N*-methyl piperazinyl in compounds **28, 35**, and **42** than pyrrolidinyl derivatives in compounds **29, 36**, and **43** (Table 2). An increase in the inhibitory activities was observed by substituting the phenol ring with two methyl as in compounds **32**, **39**, and **46** (Table 2). These data correlated with our rationale, which depends on replacing the hydroxyl group by other polar groups to prevent its phosphorylation, and this was of great importance in the design of novel SphK1 inhibitors. The effect of the nitro group in compounds **47** and **48** was the most favorable for activity and led to enhancement of both the binding free energy (Table 1) and the hydrogen bonding. In addition, substitution of the pyrazole ring with piperidine in compound **48** instead of morpholine in compound **47** decreased the inhibitory activity and the $IC_{50}$ (Table 3).

## Conclusion

Looking at the major challenges involves in the synthesis of novel inhibitors of SphK1, the current study is a first step toward the identification of different pyrazolylbenzimidazoles that could be useful in the development of potent SphK1 inhibitors. A new series of benzimidazole derivatives **26–48** was rationally designed and synthesized. Among the studied compounds, compounds **47** and **48** showed an effective binding affinity to the SphK1 and significantly inhibited SphK1. Also, the synthesized molecules were evaluated by the NCI DPT for testing their antiproliferative activity on a panel of 60 cell lines, compounds **47** and **48** exhibited an effective cytotoxic activity against several NCI cell panels. Based on molecular-docking study, most of these synthesized compounds as **47** and **48** occupy the ATP-binding pocket and existing the deep pocket of SphK1 forming several important non-covalent and hydrogen-bonding interactions with the active site residues. A considerable correlation was noticed between the docking results and the $IC_{50}$ values and its worth to mention that, compounds **47** and **48** act as promising inhibitors of SphK1 with low $IC_{50}$ values in the single digit.

## Material and methods

Luria broth and Luria agar were purchased from Himedia (Mumbai, India). Plasmid pET28b+, DH5α, and BL21-Gold cells were procured from Invitrogen (USA). Ni-NTA column was purchased from GE Healthcare (GE Healthcare Life Sciences, Uppsala, Sweden). *N*-Lauroyl sarcosine, Tris buffer, DMSO, and other reagents were purchased from Sigma Aldrich (St. Louis, MO, USA). BIOMOL® was obtained from Enzo (New York, USA). All the reagents used for buffer and chemical preparation were of analytical grade. Microanalyses and spectral data of the compounds were performed in the Microanalytical center at National Research Centre, and pharmaceutical faculty, Cairo University, Egypt, and Helmholtz Institute for Pharmaceutical Research Saarland (HIPS)—Helmholtz Centre for Infection Research (HZI), Saarbrücken, Germany. The IR spectra (4000–400 $cm^{-1}$) were recorded using KBr pellets in a Jasco FT/IR 300E Fourier transform infrared spectrophotometer on a perkin-Elemer FT-IR 1650 spectrophotometer. The $^1$H-NMR spectra were recorded using 500 and 400-MHz NMR spectrometer. Chemical shifts are reported in parts per million (ppm) from the tetramethylsilane resonance in the indicated solvent. Coupling constants (*J*) are reported in Hertz (Hz), and integration (where applicable); spectral splitting patterns are designed as follow: singlet (s); doublet (d); triplet (t); quartet (q); multiplet (m), and broad singlet (brs). The samples were referenced to the appropriate internal non-deuterated solvent peak. The data are given as follows: chemical shift ($\delta$) in ppm, multiplicity (where applicable). The mass spectra were recorded using a Finnigan mat SSQ 7000 (Thermo. Inst. Sys. Inc., USA) spectrometer at 70 eV. Chromatography solvents were HPLC grade and were used without further purification. Thin-layer chromatography (TLC) analysis was performed using Merck silica gel 60 F-254 thin-layer plates. Starting materials, reagents, and solvents for reactions were reagent grade and used as purchased. The petroleum ether had a boiling temperature in the 60–80 °C range.

### Chemistry

#### General procedure for the synthesis of compounds 26–48

These compounds were prepared by addition of a suspension of benzene-1,2-diamine derivatives **22–25** (10 mmol) and sodium metabisulfite (7.6 g, 40 mmol) dissolved in absolute ethanol (40 mL) to a solution of compounds **15–21** [52–54] (10 mmol) dissolved in absolute ethanol (30 mL). The mixture was stirred for 6–10 h and monitored by TLC. The reaction mixture was poured onto crushed ice; the resulting precipitate was collected by filtration, dried, and

**Table 4** In vitro growth inhibition % (GI%) of synthesized benzimidazole derivative against a panel of tumor cell lines at 10 μM

| Subpanel | 26 | 27 | 28 | 29 | 30 | 31 | 32 | 33 | 34 | 35 | 36 | 37 | 38 | 39 | 40 | 41 | 43 | 44 | 47 | 48 |
|---|---|---|---|---|---|---|---|---|---|---|---|---|---|---|---|---|---|---|---|---|
| Leukemia | | | | | | | | | | | | | | | | | | | | |
| CCRF-CEM | 21 | – | 41 | 13 | – | 23 | 14 | – | 21 | – | 56 | | 31 | – | – | – | – | – | 74 | 61 |
| HL-60(TB) | – | – | 21 | – | – | 10 | – | – | – | – | 22 | 41 | 11 | – | 54 | – | 12 | – | 73 | 81 |
| K-562 | – | 15 | 44 | – | 16 | 22 | 28 | – | 21 | 31 | – | 13 | 54 | – | – | 23 | – | 15 | 81 | 89 |
| MOLT-4 | – | – | 47 | 13 | 18 | 17 | 27 | – | – | – | – | 18 | 15 | – | 13 | 25 | – | 10 | 44 | 76 |
| PRMI-8226 | – | 10 | 55 | – | 18 | 19 | 23 | 11 | – | 48 | – | 29 | 27 | 14 | – | 19 | 14 | – | 65 | 68 |
| SR | – | 14 | 54 | 26 | 19 | 24 | 38 | – | – | 41 | 20 | 23 | 64 | – | 25 | 26 | – | 25 | 42 | 61 |
| Non-small cell lung cancer | | | | | | | | | | | | | | | | | | | | |
| A549/ATTC | – | – | 32 | – | 12 | – | 19 | – | – | – | 31 | 78 | 45 | – | – | – | 24 | – | 10 | 51 |
| EKVX | – | – | – | – | – | 19 | – | – | – | – | 21 | 13 | | – | – | – | – | – | 28 | 44 |
| HOP-62 | 14 | 12 | 28 | 20 | – | 13 | 12 | – | 10 | 10 | 75 | – | 23 | – | – | 10 | 10 | – | 45 | 28 |
| HOP-92 | 10 | 10 | 21 | – | – | – | 14 | 21 | 13 | 13 | 31 | 33 | – | – | – | 10 | – | – | 88 | 44 |
| NCI-H226 | 15 | – | 10 | – | – | – | – | 55 | – | – | – | 13 | – | – | 12 | – | – | – | 34 | 45 |
| NCI-H23 | 19 | 18 | – | 11 | – | – | – | – | – | – | 28 | | | – | – | – | – | – | 45 | 23 |
| NCI-H322M | – | – | 20 | – | 31 | 14 | 24 | – | 21 | – | – | 54 | 52 | 10 | – | – | 36 | – | 21 | 72 |
| NCI-H460 | – | – | 18 | – | – | – | 13 | – | – | – | 20 | | 13 | – | – | – | 3 | – | 44 | 33 |
| NCI-H522 | – | – | 24 | – | – | 13 | 41 | – | 10 | 10 | 13 | 12 | – | – | – | – | 22 | – | 19 | 16 |
| Colon cancer | | | | | | | | | | | | | | | | | | | | |
| COLO 205 | 11 | – | – | – | 20 | – | 25 | – | – | – | – | | 12 | – | – | – | – | – | 21 | 41 |
| HCC-2998 | – | – | – | – | – | – | – | – | – | – | – | 23 | | – | – | – | – | – | 70 | 52 |
| HCT-116 | 10 | 17 | 27 | – | 19 | 26 | 33 | – | 21 | – | – | – | 13 | – | – | 19 | – | – | 15 | 15 |
| HCT-15 | – | – | 24 | – | – | 11 | 11 | – | 13 | – | – | – | 12 | – | – | – | – | – | 22 | 18 |
| HT29 | – | – | 17 | – | – | – | nd | – | 28 | – | – | 13 | 10 | – | – | – | – | – | 10 | 42 |
| KM12 | – | – | 26 | – | – | – | 14 | – | 10 | – | – | – | – | – | – | – | – | – | 25 | 12 |
| SW-620 | – | – | – | – | – | – | – | – | 11 | – | – | – | 56 | – | – | – | – | – | 35 | 17 |
| CNS cancer | | | | | | | | | | | | | | | | | | | | |
| SF-268 | – | – | 22 | – | 10 | 11 | 10 | – | – | – | – | 44 | 13 | 12 | – | – | – | – | 10 | 11 |
| SF-295 | – | – | 16 | – | – | – | – | – | – | – | – | 13 | 30 | – | – | – | – | – | 10 | 10 |
| SF-539 | – | – | 37 | – | – | – | – | – | – | 42 | – | – | 51 | – | – | – | – | – | 20 | 43 |
| SNB-19 | – | – | – | – | – | – | – | – | – | – | – | 45 | 13 | – | – | – | – | – | 40 | 11 |
| SNB-75 | 20 | 16 | 50 | – | 14 | 14 | 12 | – | 15 | 15 | 18 | – | – | – | 13 | – | – | – | 09 | 24 |
| U251 | 14 | 11 | 30 | – | – | – | 10 | – | – | – | – | – | – | – | – | – | – | – | 43 | 11 |
| Melanoma | | | | | | | | | | | | | | | | | | | | |
| LOX IMVI | – | 11 | 21 | – | 11 | 15 | 11 | – | – | – | – | | | 12 | – | 10 | – | – | 45 | 18 |
| MALME-3M | 11 | – | 14 | 19 | – | – | 13 | 54 | – | 13 | 23 | | 31 | 75 | – | – | – | – | 21 | 31 |
| M14 | – | – | 21 | – | 11 | – | – | – | – | – | 10 | | | 22 | – | – | – | – | 42 | 24 |
| MDA-MB-435 | – | – | 27 | 21 | – | – | – | 42 | 21 | – | 46 | | 11 | – | – | – | 82 | – | 37 | 12 |
| SK-MEL-2 | – | – | – | – | – | – | 22 | 74 | – | – | 28 | 2 | 31 | – | – | – | – | – | – | 12 |
| SK-MEL-28 | – | – | 15 | – | – | – | – | – | – | – | 64 | | | – | – | – | 45 | – | 45 | 75 |
| SK-MEL-5 | – | – | 25 | – | – | – | – | – | – | – | 59 | | | – | – | – | – | – | 55 | 77 |
| UACC-257 | – | – | – | – | – | – | – | – | – | – | 10 | | | – | – | – | – | – | – | 14 |
| UACC-62 | – | 28 | 32 | 15 | 23 | 23 | 43 | – | 11 | 11 | 10 | | | 21 | 14 | 30 | 19 | 20 | 16 | 37 |
| Ovarian cancer | | | | | | | | | | | | | | | | | | | | |
| IGROV1 | 13 | 20 | 11 | – | 31 | 33 | 51 | – | – | – | – | 13 | | – | – | 26 | 15 | – | 24 | 17 |
| OVCAR-3 | 19 | 10 | 23 | – | 11 | 13 | 23 | 31 | – | – | – | – | 10 | – | – | – | – | – | 25 | 35 |
| OVCAR-4 | 25 | 13 | 15 | – | 13 | 16 | 21 | – | 25 | – | – | | | – | – | 14 | – | 14 | 21 | 18 |
| OVCAR-5 | – | 29 | – | – | – | – | 16 | 22 | 12 | – | – | | 64 | – | – | – | – | – | 14 | 55 |

**Table 4** (continued)

| Subpanel | 26 | 27 | 28 | 29 | 30 | 31 | 32 | 33 | 34 | 35 | 36 | 37 | 38 | 39 | 40 | 41 | 43 | 44 | 47 | 48 |
|---|---|---|---|---|---|---|---|---|---|---|---|---|---|---|---|---|---|---|---|---|
| OVCAR-8 | 31 | – | 44 | – | – | 11 | 12 | 46 | – | – | – | 23 | | – | – | – | – | – | 34 | 74 |
| NCI/ADR-RES | – | 10 | 11 | 45 | 78 | – | 10 | – | 46 | 13 | – | 23 | 64 | – | – | 10 | – | 12 | 22 | 10 |
| SK-OV-3 | 45 | – | 45 | – | – | 11 | 14 | – | – | – | – | 12 | 76 | – | – | 12 | – | – | 37 | 45 |
| Renal cancer | | | | | | | | | | | | | | | | | | | | |
| 786-0 | – | – | 16 | – | – | – | 12 | 74 | – | – | 33 | 27 | 13 | – | – | – | – | – | – | 28 |
| A498 | 29 | 44 | 43 | 30 | 35 | 45 | 48 | – | – | 31 | 21 | 45 | 10 | 29 | 30 | 39 | 32 | 39 | 23 | 46 |
| ACHN | 13 | 10 | 32 | – | – | 10 | 14 | – | 13 | 31 | 81 | 64 | 41 | – | 10 | 14 | – | – | 72 | 71 |
| CAKI-1 | 24 | 29 | 37 | 21 | 40 | 35 | 58 | 31 | 18 | 18 | 20 | 31 | 21 | 23 | 17 | 33 | 14 | 13 | 20 | 27 |
| RXF 393 | – | – | 35 | – | – | – | – | 27 | – | – | – | 74 | 31 | – | – | – | – | – | 31 | 17 |
| SN 12C | 21 | – | 16 | – | 31 | 12 | – | 75 | – | 11 | – | 20 | 46 | – | – | – | – | – | 22 | 22 |
| TK-10 | – | – | 12 | – | – | – | nd | – | – | – | – | | | – | – | – | – | – | – | 10 |
| UO-31 | 30 | 29 | 35 | 24 | 33 | 38 | 37 | 19 | 21 | 21 | 13 | 27 | 31 | 30 | 25 | 24 | 29 | 26 | 18 | 27 |
| Prostate cancer | | | | | | | | | | | | | | | | | | | | |
| PC-3 | 13 | 17 | 39 | – | 18 | 17 | 23 | 87 | 10 | 10 | – | 34 | 31 | 13 | – | 19 | 14 | – | – | 24 |
| DU-145 | – | – | 16 | – | – | – | – | 31 | – | 27 | – | 78 | 54 | – | – | – | – | – | – | 35 |
| Breast cancer | | | | | | | | | | | | | | | | | | | | |
| MCF7 | – | – | 21 | – | – | – | – | – | – | – | 10 | 13 | | – | – | – | – | – | 75 | 67 |
| MDA-MB-231/ ATTC | – | 16 | 15 | – | 13 | 27 | 21 | 23 | 31 | 54 | – | 58 | 23 | 56 | 10 | 21 | 11 | – | 57 | 24 |
| BT-549 | – | – | 23 | – | – | 10 | – | – | – | – | – | 46 | 18 | – | – | – | – | – | 73 | 47 |
| T-47D | 12 | 19 | 54 | 16 | 25 | 26 | 28 | – | – | – | 12 | 22 | 31 | – | – | 13 | 10 | – | 83 | 26 |
| MDA-MB-468 | 29 | 25 | 22 | 13 | – | – | 17 | – | 13 | – | – | 47 | 20 | – | – | – | – | – | 75 | 64 |

recrystallized from ethanol to give compounds **26–48**, which characterized by IR, 1H- NMR, 13C- NMR, MS, and elemental analyses.

**2-(3-Methyl-5-morpholino-1-phenyl-1H-pyrazol-4-yl)-1H-benzo[*d*]imidazole (26)** White solid; 81% yield; mp: 258–260 °C; IR (KBr) $\upsilon_{max}$: 3470 (NH), 3058, 2947, 1627 (C=N), 1593 (C=C) $cm^{-1}$; $^{1}$H-NMR (DMSO-$d_6$, 500 MHz): $\delta = 2.25$ (3H, s, $CH_3$), 2.90 (4H, m, H-3, H-5 morpholine protons,), 3.49 (4H, m, H-2, H-6 morpholine protons), 7.20 (2H, m, Ar–H), 7.40 (1H, m, Ar–H), 7.52 (3H, m, Ar–H), 7.67 (d, $J = 7.5$ Hz, 1H, Ar–H), 7.73 (d, $J = 7.5$ Hz, 2H, Ar–H), 12.34 (1H, s, NH); $^{13}$C-NMR (DMSO-$d_6$, 125 MHz): $\delta = 13.4$ ($CH_3$), 50.5, 66.5, 104.0, 112.0, 119.1, 122.3, 123.1, 124.7, 128.2, 129.8, 134.7, 139.5, 143.6, 146.1(C–N), 148.4 (C=N), 149.4 (C–O); MS (EI,70 Ev): *m/z* (%) 360 $[M + 1]^+$ (100); Anal. Calcd for $C_{21}H_{21}N_5O$: C, 70.17; H, 5.89; N, 19.48. Found: C, 70.35; H, 5.76; N, 19.54.

**2-(3-Methyl-1-phenyl-5-(piperidin-1-yl)-1H-pyrazol-4-yl)-1H-benzo[*d*]imidazole (27)** White solid; 81% yield; mp: 218–220 °C; IR (KBr) $\upsilon_{max}$: 3426 (NH), 3061, 2927, 1627 (C=N), 1594 (C=C) $cm^{-1}$; $^{1}$H-NMR (DMSO-$d_6$, 500 MHz): $\delta = 1.37$ (6H, brs, H-3, H-4, H-5 piperidine protons), 2.21 (3H, s, $CH_3$), 2.84 (4H, s, H-2, H-6 piperidine protons,), 7.19 (2H, m, Ar–H), 7.36 (1H, m, Ar–H), 7.51 (2H, m, Ar–H), 7.59 (2H, brs, Ar–H), 7.72 (d, $J = 8.0$ Hz, 2H, Ar–H), 12.19 (1H, brs, NH); $^{13}$C-NMR (DMSO-$d_6$, 125 MHz): $\delta = 13.1$ ($CH_3$), 23.3, 25.2, 51.0, 103.4, 121.6, 123.7, 127.0, 128.9, 139.5, 146.1, 147.5 (C–N), 149.9 (C=N); MS (EI,70 Ev): *m/z* (%) 358.21 $[M + 1]^+$ (100); Anal. Calcd for $C_{22}H_{23}N_5$: C, 73.92; H, 6.49; N, 19.59. Found: C, 73.85; H, 6.61; N, 19.67.

**2-(3-Methyl-5-(4-methylpiperazin-1-yl)-1-phenyl-1H-pyrazol-4-yl)-1H-benzo[*d*]-imidazole (28)** Brown solid; 50% yield; mp: 236–238 °C; IR (KBr) $\upsilon_{max}$: 3424 (NH), 3069, 2925, 1630 (C=N), 1589 (C=C) $cm^{-1}$; $^{1}$H-NMR (DMSO-$d_6$, 500 MHz): $\delta = 2.27$ (3H, s, $CH_3$), 2.60 (3H, s, $CH_3$), 2.85 (4H, s, piperazine protons), 3.11 (4H, s, piperazine protons), 7.22 (2H, s, Ar–H), 7.43 (d, $J = 9.0$ Hz,1H, Ar–H), 7.54 (2H, m, Ar–H), 7.61 (2H, s, Ar–H), 7.71 (d, $J = 9.5$ Hz, 2H, Ar–H), 12.41 (1H, brs, NH); $^{13}$C-NMR (DMSO-$d_6$, 125 MHz): $\delta = 13.7$ ($CH_3$), 43.1 ($CH_3$), 47.5 (CH-3 + CH-5 piperazine carbons), 53.5 (CH-3 + CH-5

**Table 5** Docking results for compounds **26–48** docked by AutoDock vina tool into SphK1 kinase (PDB ID: 4V24) in comparison to the co-crystallized PF-543 ligand

| Compound no. | Interaction type | No. of interactions | Interacting residues |
|---|---|---|---|
| **26** | van der Waals | 11 | Phe173, Asp178, Phe192, Thr196, Leu259, Leu261, Ala274, Phe288, Val290, Leu299, His311 |
| | Hydrogen bond | 1 | Thr196 |
| | π–sigma | 2 | Ile174, Leu302 |
| | π–sulfur | 1 | Met306 |
| | π–π stacked | 1 | Phe303 |
| | π–alkyl | 3 | Val177, Leu268, Leu319 |
| **27** | van der Waals | 8 | Phe173, Asp178, Phe192, Thr196, Leu261, Phe288, Leu299, His311 |
| | π-sigma | 2 | Ile174, Leu302 |
| | π–sulfur | 1 | Met306 |
| | π–π stacked | 1 | Phe303 |
| | π–alkyl | 6 | Val177, Leu259, Leu268, Ala274, Val290, Leu319 |
| **28** | van der Waals | 10 | Phe173, Asp178, Phe192, Thr196, Leu259, Leu261, Ala274, Phe288, Leu299, His311 |
| | Hydrogen bond | 1 | Thr196 |
| | π–sigma | 2 | Ile174, Leu302 |
| | π–sulfur | 1 | Met306 |
| | π–π stacked | 1 | Phe303 |
| | π–alkyl | 4 | Val177, Leu268, Val290, Leu319 |
| **29** | van der Waals | 7 | Phr173, Asp178, Phe192, Thr196, Leu261, Leu299, His311 |
| | π–sigma | 2 | Ile174, Leu302 |
| | π–sulfur | 1 | Met306 |
| | π–π stacked | 1 | Phe303 |
| | π–alkyl | 5 | Val177, Leu259, Leu268, Ala274, Val290 |
| **30** | van der Waals | 1 | Ile274 |
| | π–anion | 1 | Asp178 |
| | π–π t shaped | 1 | Phe192 |
| | π–alkyl | 1 | Leu268 |
| **31** | van der Waals | 14 | Phe173, Asp178, Phe192, Thr196, Leu259, Leu261, Met272, Ala274, Phe288, Val290, Leu302, Phe303, His311, Leu319 |
| | π–sigma | 1 | Ile174 |
| | π–sulfur | 1 | Met306 |
| | π–alkyl | 2 | Val177, Leu268 |
| **32** | van der Waals | 7 | Phe173, Asp178, Phe192, Thr196, Leu259, Leu261, Val290 |
| | π–sigma | 1 | Ile174 |
| | π–sulfur | 1 | Met306 |
| | π–alkyl | 7 | Val177, Leu268, Ala274, Phe288, Leu302, His311, Leu319 |
| **33** | van der Waals | 11 | Phe173, Asp178, Phe192, Thr196, Leu259, Leu261, Ala274, Phe288, Val290, Leu299, His311 |
| | Hydrogen bond | 2 | Thr196, Leu268 |
| | π–sigma | 2 | Ile174, Leu302 |
| | π–sulfur | 1 | Met306 |

**Table 5** (continued)

| Compound no. | Interaction type | No. of interactions | Interacting residues |
|---|---|---|---|
| | π–π stacked | 1 | Phe303 |
| | π–alkyl | 2 | Val177, Leu319 |
| **34** | van der Waals | 8 | Phe173, Asp178, Phe192, Thr196, Leu261, Phe288, Leu299, His311 |
| | Hydrogen bond | 1 | Thr196 |
| | Unfavorable | 1 | Leu268 |
| | π–sigma | 2 | Ile274, Leu302 |
| | π–sulfur | 1 | Met306 |
| | π–π stacked | 1 | Phe303 |
| | π–alkyl | 5 | Val177, Leu259, Ala274, Val290, Leu319 |
| **35** | van der Waals | 11 | Phe173, Asp178, Thr196, Leu259, Leu261, Gly269, Met272, Ala274, Phe288, Leu299, His311 |
| | π–sigma | 2 | Ile174, Leu302 |
| | π–sulfur | 1 | Met306 |
| | π–π stacked | 2 | Phe192, Phe303 |
| | π–alkyl | 4 | Val177, Leu268, Val290, Leu319 |
| **36** | van der Waals | 8 | Ala115, Phe173, Asp178, Phe192, Thr196, Leu261, Leu299, His311 |
| | Hydrogen bond | 2 | Thr196, Leu268 |
| | π–sigma | 3 | Ile174, Leu302, Phe303 |
| | π–sulfur | 1 | Met306 |
| | π–π stacked | 1 | Phe303 |
| | π–alkyl | 5 | Val177, Leu259, Ala274, Val290, Leu319 |
| **37** | van der Waals | 10 | Phe173, Asp178, Phe192, Thr196, Leu259, Leu261, Gly269, Met272, Val290, Phe303 |
| | π–sigma | 1 | Ile174 |
| | π–sulfur | 1 | Met306 |
| | π–alkyl | 7 | Val177, Leu268, Ala274, Phe288, Leu302, His311, Leu319 |
| **38** | van der Waals | 16 | Ala115, Phe173, Asp178, Phe192, Thr196, Leu259, Leu261, Gly269, Met272, Ala274, Phe288, Val290, Leu302, Phe303, His311, Leu319 |
| | Hydrogen bond | 1 | Leu268 |
| | π–sigma | 1 | Ile174 |
| | π–sulfur | 1 | Met306 |
| | π–alkyl | 1 | Val177 |
| **39** | van der Waals | 11 | Ala115, Phe173, Asp178, Phe192, Thr196, Leu259, Leu261, Leu263, Gly268, Val290, Phe303 |
| | Hydrogen bond | 2 | Thr196, Leu268 |
| | π–sigma | 1 | Ile174 |
| | π–sulfur | 1 | Met306 |
| | π–alkyl | 6 | Val177, Ala274, Phe288, Leu302, His311, Leu319 |
| **40** | van der Waals | 11 | Phe173, Asp178, Phe192, Thr196, Leu259, Leu261, Ala274, Phe288, Val290, Leu299, His311 |
| | Hydrogen bond | 1 | Thr196 |
| | π–sigma | 2 | Ile174, Leu302 |
| | π–sulfur | 1 | Met306 |
| | π–π stacked | 1 | Phe303 |

**Table 5** (continued)

| Compound no. | Interaction type | No. of interactions | Interacting residues |
|---|---|---|---|
| | π–alkyl | 3 | Val177, Leu268, Leu319 |
| **41** | van der Waals | 8 | Phe173, Asp178, Phe192, Thr196, Leu261, Phe288, Leu299, His311 |
| | π–sigma | 2 | Ile174, Leu302 |
| | π-sulfur | 1 | Met306 |
| | π–π stacked | 1 | Phe303 |
| | π–alkyl | 6 | Val177, Leu259, Leu268, Ala274, Val290, Leu319 |
| **42** | van der Waals | 10 | Phe173, Asp178, Thr196, Leu259, Leu261, Met272, Ala274, Phe288, Leu299, His311 |
| | Hydrogen bond | 1 | Thr196 |
| | π–sigma | 3 | Ile174, Phe192, Leu302 |
| | π–sulfur | 1 | Met306 |
| | π–π stacked | 1 | Phe303 |
| | π–alkyl | 4 | Val177, Leu268, Val290, Leu319 |
| **43** | van der Waals | 7 | Phe173, Asp178, Phe192, Thr196, Leu261, Leu299, His311 |
| | π–sigma | 3 | Ile174, Leu302, Phe303 |
| | π–π stacked | 1 | Phe303 |
| | π–alkyl | 5 | Val177, Leu259, Leu268, Ala274, Leu319 |
| **44** | van der Waals | 8 | Phe173, Asp178, Thr196, Leu259, Leu261, Met272, Val290, Phe303 |
| | π–sigma | 2 | Ile174, Phe192 |
| | π–sulfur | 1 | Met306 |
| | π–alkyl | 7 | Val177, Leu268, Ala274, Phe288, Leu302, His311, Leu319 |
| **45** | van der Waals | 12 | Phe173, Asp178, Thr196, Leu259, Leu261, Met272, Ala274, Phe288, Val290, Leu302, His311, Leu319 |
| | π–sigma | 2 | Ile174, Phe192 |
| | π–sulfur | 1 | Met306 |
| | π–alkyl | 2 | Val177, Leu268 |
| **46** | van der Waals | 9 | Phe173, Asp178, Thr196, Leu259, Leu261, Leu263, Met272, Val290, Phe303 |
| | π–sigma | 2 | Ile174, Phe192 |
| | π–sulfur | 1 | Met306 |
| | π–alkyl | 7 | Val177, Leu268, Ala274, Phe288, Leu302, His311, Leu319 |
| **47** | van der Waals | 10 | Phe173, Asp178, Phe192, Thr196, Leu259, Leu261, Ala274, Phe288, Leu299, His311 |
| | Hydrogen bond | 1 | Thr196 |
| | π–sigma | 2 | Ile174, Leu302 |
| | π–π interaction | 1 | Phe303 |
| | π–sulfur | 1 | Met306 |
| | π–alkyl | 4 | Val177, Leu268, Val290, Leu319 |
| **48** | van der Waals | 9 | Phe173, Asp178, Phe192, Thr196, Leu261, Phe288, Val290, Leu299, His311 |
| | Hydrogen bond | 1 | Thr196 |
| | π–sigma | 2 | Ile174, Leu302 |
| | π–sulfur | 1 | Met306 |

**Table 5** (continued)

| Compound no. | Interaction type | No. of interactions | Interacting residues |
|---|---|---|---|
| | π–π interaction | 1 | Phe303 |
| | π–alkyl | 5 | Val177, Leu268, Leu259, Ala274, Leu319 |
| **PF-543**[a] | van der Waals | 11 | Leu167, Ser168, Ala170, Leu259, Leu261, Phe288, Val290, Leu302, Met306, Ala339, Gly342 |
| | Hydrogen bond | 3 | Asp178, Thr196, His311 |
| | π–sigma | 1 | Phe192 |
| | π–alkyl | 8 | Phe173, Ile174, Val177, Leu200, Leu268, Ala274, Leu299, Leu319 |
| | π–π stacked | 2 | Phe192, Phe303 |
| | π–sulfur | 1 | Met272 |

[a]Native ligand: ((r)-1-(4-((3-methyl-5-((phenylsulfonyl)methyl)phenoxy)methyl)benzyl)pyrrolidin-2-yl)methanol

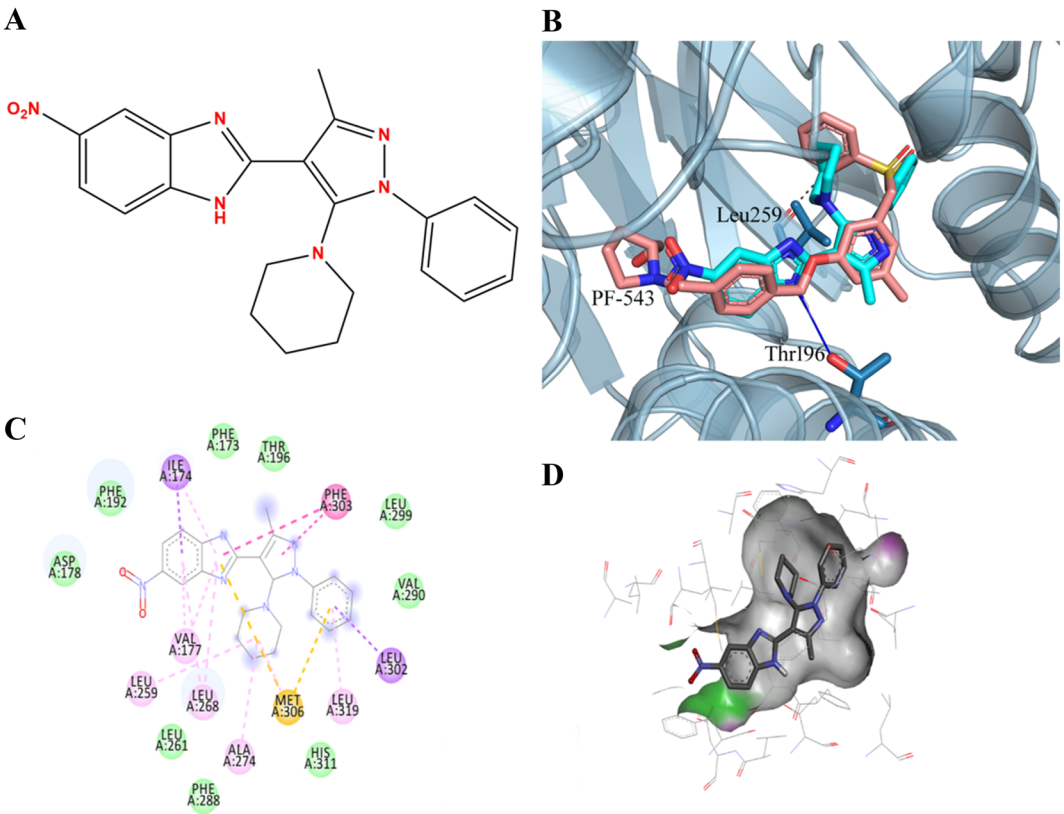


**Fig. 7** Compound **48** binding to SphK1. **A** Chemical structure of compound **48**. **B** Graphical representation of PF-543 aligned with compound **48** interacting with binding site residues of SphK1. **C** 2D scheme of protein–ligand interactions. **D** Surface view of SphK1 binding pocket occupied by compound **48**

piperazine carbons), 105.2, 123.7, 124.5, 125.7, 127.9, 129.9, 131.5, 139.4, 145.5; MS (EI,70 Ev): *m/z* (%) 372.21 $[M]^+$ (100); 373.21$[M+1]^+$ (25); Anal. Calcd for $C_{22}H_{24}N_6$: C, 70.94; H, 6.49; N, 22.56. Found: C, 70.82; H, 6.57; N, 22.43.

**2-(3-Methyl-1-phenyl-5-(pyrrolidin-1-yl)-1H-pyrazol-4-yl)-1H-benzo[*d*]imidazole (29)** Buff solid; 64% yield; mp: 241–243 °C; IR (KBr) $\upsilon_{max}$: 3423 (NH), 3060, 2958, 1622 (C=N), 1589 (C=C) $cm^{-1}$; $^1$H-NMR (DMSO-$d_6$, 500 MHz): $\delta = 1.70$ (4H, m, H-3, H-4 pyrrolidine protons), 2.20 (3H, s, $CH_3$), 2.95 (4H, m, H-2, H-5 pyrrolidine protons), 7.17 (2H, m, Ar–H), 7.38 (1H, m, Ar–H), 7.50 (2H, m, Ar–H), 7.57 (4H, m, Ar–H), 12.30 (1H, brs, NH); $^{13}$C-NMR (DMSO-$d_6$, 125 MHz): $\delta = 13.2$ ($CH_3$), 25.170 (CH-3, CH-4 of pyrrolidine carbons), 50.4 (CH-2, CH-5 of

pyrrolidine carbons), 101.0, 121.5, 124.2, 127.1, 129.0, 140.0, 146.5 (C–N), 147.7 (C–N), 147.8 (C= N); MS (EI,70 Ev): *m/z* (%) 344.2 $[M + 1]^+$ (100), 345.2 $[M + 2]^+$ (25); Anal. Calcd for $C_{21}H_{21}N_5$: C 73.44; H, 6.16; N, 20.39. Found: C, 73.25; H, 6.29; N, 20.45.

**2-(3-Methyl-5-phenoxy-1-phenyl-1H-pyrazol-4-yl)-1H-benzo[*d*]imidazole (30)** Pale yellow solid; 79% yield; mp: 97–99 °C; IR (KBr) $\upsilon_{max}$: 3424 (NH), 3069, 2925, 1630 (C=N), 1589 (C=C) $cm^{-1}$; $^1$H-NMR (DMSO-$d_6$, 500 MHz): $\delta = 2.63$ (3H, s, $CH_3$), 6.94 (3H, m, Ar–H), 7.13 (2H, m, Ar–H), 7.21 (2H, m, Ar–H), 7.32 (1H, m, Ar–H), 7.48 (4H, m, Ar–H), 7.66 (d, $J = 7.5$ Hz, 2H, Ar–H), 12.14 (1H, brs, NH); $^{13}$C-NMR (DMSO-$d_6$, 125 MHz): $\delta = 14.6$ ($CH_3$), 101.5, 115.4, 121.7, 122.1, 123.7, 127.5, 129.4, 129.9, 137.1, 144.1, 146.1(C–N), 148.2 (C=N), 155.8 (C–O); MS (EI, 70 Ev): *m/z* (%) 367.1 $[M + 1]^+$ (100), 368.2 $[M]^+$ (25); Anal. Calcd for $C_{23}H_{18}N_4O$: C, 75.39; H, 4.95; N, 15.29. Found: C, 75.25; H, 4.80; N, 15.40.

**2-(3-Methyl-1-phenyl-5-(pyridin-2-yloxy)-1H-pyrazol-4-yl)-1H-benzo[*d*]-imidazole (31)** Buff solid; 56% yield; mp: 114–117 °C; IR (KBr) $\upsilon_{max}$: 3424 (NH), 3069, 2925, 1630 (C=N), 1589 (C=C) $cm^{-1}$; $^1$H-NMR (DMSO-$d_6$, 500 MHz): $\delta = 2.62$ (3H, s, $CH_3$), 7.10 (2H, m, Ar–H), 7.14 (2H, m, Ar–H), 7.20 (2H, m, Ar–H), 7.32 (1H, m, Ar–H), 7.45 (2H, m, Ar–H), 7.52 (2H, m, Ar–H), 7.65 (d, $J =$ 8.0 Hz, 2H, Ar–H), 12.36 (1H, brs, NH); $^{13}$C-NMR (DMSO-$d_6$, 125 MHz): $\delta = 14.6$ ($CH_3$), 101.1, 115.4, 121.9, 122.2, 123.8, 127.5, 129.4, 129.9, 137.1, 143.9, 145.2 (C–N), 148.2 (C=N), 155.8 (C–O); MS (EI,70 Ev): *m/z* (%) 367.1 $[M]^+$ (100), 368.2 $[M + 1]^+$ (25); Anal. Calcd for $C_{22}H_{17}N_5O$: C, 71.92; H, 4.66; N, 19.06. Found: C, 71.76; H, 4.53; N, 19.19.

**2-(5-(2,5-Dimethylphenoxy)-3-methyl-1-phenyl-1H-pyrazol-4-yl)-1H-benzo[*d*]- imidazole (32)** White solid; 72% yield; mp: 102–104 °C; IR (KBr) $\upsilon_{max}$: 3441 (NH), 3069, 2856, 1625 (C=N), 1594 (C=C) $cm^{-1}$; $^1$H-NMR (DMSO-$d_6$, 500 MHz): $\delta = 1.97$ (3H, s, $CH_3$), 2.34 (3H, s, $CH_3$), 2.60 (3H, s, $CH_3$), 6.28 (1H, s, Ar–H), 6.63 (d, $J = 7.5$ Hz, 1H, Ar–H), 7.00 (d, $J = 7.5$ Hz, 1H, Ar–H), 7.14 (2H, m, Ar–H), 7.32 (1H, m, Ar–H), 7.44 (2H, m, Ar–H), 7.51 (2H, m, Ar–H), 7.58 (d, $J = 8.0$ Hz, 2H, Ar–H), 12.07 (1H, brs, NH); $^{13}$C-NMR (DMSO-$d_6$, 125 MHz): $\delta = 14.5$ ($CH_3$), 15.6 ($CH_3$), 20.5 ($CH_3$), 101.3, 113.4, 121.7, 122.5, 123.2, 124.1, 127.8, 129.2, 131.0, 136.4, 137.2, 144.2, 146.6 (C–N), 148.0 (C=N), 154.0 (C–O); MS (EI,70 Ev): *m/z* (%) 395.2 $[M + 1]^+$ (100), 396.2 $[M + 2]^+$ (25); Anal. Calcd for $C_{25}H_{22}N_4O$: C, 76.12; H, 5.62; N, 14.20. Found: C, 76.31; H, 5.73; N, 14.41.

**2-(3-Methyl-5-morpholino-1-phenyl-1H-pyrazol-4-yl)-1H-benzo[*d*]imidazole-5-carboxylic acid (33)** White solid; 73% yield; mp: 192–194 °C; IR (KBr) $\upsilon_{max}$: 3423 (NH), 3097, 2966, 2855 (OH), 1627 (C=N), 1590 (C=C), 1693 (C=O) $cm^{-1}$; $^1$H-NMR (DMSO-$d_6$, 400 MHz): $\delta = 2.29$ (3H, s, $CH_3$), 2.93 (4H, s, H-3, H-5 morpholine protons), 3.50 (4H, s, H-2, H-6 morpholine protons), 7.41 (1H, m, Ar–H), 7.54 (2H, m, Ar–H), 7.70 (3H, m, Ar–H), 7.85 (d, $J = 7.2$ Hz, 1H, Ar–H), 8.21 (1H, s, Ar–H), 12.63 (1H, brs); $^{13}$C-NMR (DMSO-$d_6$, 125 MHz): $\delta = 13.3$ ($CH_3$), 50.0, 65.9, 103.7, 123.4, 124.2, 127.5, 129.0, 139.1, 147.5 (C–N), 148.9 (C=N), 167.9 (C=O); MS (EI,70 Ev): *m/z* (%) 404.0 $[M + 1]^+$ (100); Anal. Calcd for $C_{22}H_{21}N_5O_3$: C, 65.50; H, 5.25; N, 17.36. Found: C, 65.65; H, 5.42; N, 17.47.

**2-(3-Methyl-1-phenyl-5-(piperidin-1-yl)-1H-pyrazol-4-yl)-1H-benzo[*d*]imidazole-5-carboxylic acid (34)** White solid; 80% yield; mp: 156–158 °C; IR (KBr) $\upsilon_{max}$: 3427 (NH), 3088, 2924, 1833 (C=O), 1626 (C=N), 1596 (C=C) $cm^{-1}$; $^1$H-NMR (DMSO-$d_6$, 400 MHz): $\delta = 1.36$ (6H, m, H-3, H-4, H-5 piperidine protons), 2.23 (s, 3H, $CH_3$), 2.83 (4H, m, H-2, H-6 piperidine protons), 7.38 (1H, m, Ar–H), 7.52 (2H, m, Ar–H), 7.67 (3H, m, Ar–H), 7.84 (d, $J = 8.0$ Hz, 1H, Ar–H), 8.21 (1H, s, Ar–H), 12.69 (1H, brs); $^{13}$C-NMR (DMSO-$d_6$, 125 MHz): $\delta = 13.2$ ($CH_3$), 23.3 (CH-4 of piperidine carbons), 25.2 (CH-3, CH-5 of piperidine carbons), 51.0 (CH-2, CH-6 of piperidine carbons), 103.0, 123.9, 127.2, 129.0, 139.4, 147.4 (C=N), 150.1 (C–O), 167.9 (C=O); MS (EI,70 Ev): *m/z* (%) 402.2 $[M + 1]^+$ (100); Anal. Calcd for $C_{23}H_{23}N_5O_2$: C, 68.81; H, 5.77; N, 17.44. Found: C, 68.95; H, 5.76; N, 17.59.

**2-(3-Methyl-5-(4-methylpiperazin-1-yl)-1-phenyl-1H-pyrazol-4-yl)-1H-benzo[*d*]- imidazole-5-carboxylic acid (35)** Brown solid; 42% yield; mp: 289–291 °C; IR (KBr) $\upsilon_{max}$: 3439 (NH), 3066, 2962, 1689 (C=O), 1625 (C=C), 1594 (C=C) $cm^{-1}$; $^1$H-NMR (DMSO-$d_6$, 500 MHz): $\delta = 2.11$ (3H, s, $CH_3$), 2.24 (7H, m, $CH_3 + 4$H piperazine protons), 2.92 (4H, m, piperazine protons), 7.39 (1H, m, Ar–H), 7.51 (2H, m, Ar–H), 7.64 (d, $J = 8.5$ Hz, 1H, Ar–H), 7.69 (d, $J = 7.5$ Hz, 2H, Ar–H), 7.84 (d, $J = 8.5$ Hz, 1H, Ar–H), 8.20 (1H, s, Ar–H), 12.63 (1H, brs); $^{13}$C-NMR (DMSO-$d_6$, 125 MHz): $\delta = 13.6$ ($CH_3$), 40.0 (N–$CH_3$), 48.6 (CH-3 + CH-5 piperazine carbons), 53.9 (CH-2 + CH-6 piperazine carbons), 103.7, 125.1, 128.9, 130.3, 139.4, 148.0(C–N), 149.0 (C=N), 149.2 (C=N), 170.9 (C=O); MS (EI,70 Ev): *m/z* (%) 417.2 $[M + 1]^+$ (50); Anal. Calcd for $C_{23}H_{24}N_6O_2$: C, 66.33; H, 5.81; N, 20.18. Found: C, 66.49; H, 5.72; N, 20.27.

**2-(3-Methyl-1-phenyl-5-(pyrrolidin-1-yl)-1H-pyrazol-4-yl)-1H-benzo[*d*]-imidazole-5-carboxylic acid (36)** Buff solid; 51% yield; mp: 169–171 °C; IR (KBr) $\upsilon_{max}$: 3423 (NH), 3060, 2927, 1695 (C=O), 1624 (C=N), 1542 (C=C) $cm^{-1}$;

$^1$H-NMR (DMSO-$d_6$, 500 MHz): $\delta = 1.71$ (4H, m, H-3, H-4 pyrrolidine protons), 2.23 (3H, s, $CH_3$), 2.96 (4H, m, H-2, H-5 pyrrolidine protons), 7.40 (1H, m, Ar–H), 7.50 (2H, m, Ar–H), 7.56 (d, $J = 7.0$ Hz, 2H, Ar–H), 7.62 (d, $J = 8.5$ Hz, 1H, Ar–H), 7.82 (dd, 1H, $J = 8.5$ Hz, $J = 1.5$ Hz, Ar–H), 8.16 (1H, s, Ar–H), 12.60 (1H, brs); $^{13}$C-NMR (DMSO-$d_6$, 125 MHz): $\delta = 13.3$ ($CH_3$), 25.3 (CH-3, CH-4 of pyrrolidine carbons), 51.1 (CH-2, CH-5 of pyrrolidine carbons), 100.5, 125.1, 127.4, 129.1, 141.0, 147.5 (C=N), 168.2 (C=O); MS (EI,70 Ev): *m/z* (%) 388.1 $[M + 1]^+$ (100); Anal. Calcd for $C_{22}H_{21}N_5O_2$: C, 68.20; H, 5.46; N, 18.08. Found: C, 68.35; H, 5.65; N, 18.26.

**2-(3-Methyl-5-phenoxy-1-phenyl-1H-pyrazol-4-yl)-1H-benzo[*d*]-imidazole-5-carboxylic acid (37)** Buff solid, 75% yield; mp: 138–140 °C; IR (KBr) $\upsilon_{max}$: 3435 (NH), 3066, 2927, 1690 (C=O), 1629 (C=N), 1594 (C=C) cm$^{-1}$; $^1$H-NMR (DMSO-$d_6$, 400 MHz): $\delta = 2.62$ (3H, s, $CH_3$), 6.96 (3H, m, Ar–H), 7.22 (2H, m, Ar–H), 7.35 (1H, m, Ar–H), 7.47 (3H, m, Ar–H), 77.67 (2H, m, Ar–H), 7.75 (1H, s, Ar–H), 8.17 (1H, s, Ar–H), 12.37 (1H, s); MS (EI,70 Ev): *m/z* (%) 411.1 $[M + 1]^+$ (100), 412.2 $[M + 2]^+$ (25); Anal. Calcd for $C_{24}H_{18}N_4O_3$: C, 70.23; H, 4.42; N, 13.65. Found: C, 70.33; H, 4.35; N, 13.71.

**2-(3-Methyl-1-phenyl-5-(pyridin-2-yloxy)-1H-pyrazol-4-yl)-1H-benzo[*d*]- imidazole-5-carboxylic acid (38)** Pale brown powder; 55% yield; mp: 147–150 °C; IR (KBr) $\upsilon_{max}$: 3424 (NH), 3069, 2925, 1630 (C=N), 1589 (C=C) cm$^{-1}$; $^1$H-NMR (DMSO-$d_6$, 400 MHz): $\delta = 2.65$ (3H, s, $CH_3$), 6.95 (3H, m, Ar–H), 7.21 (2H, m, Ar–H), 7.33 (1H, m, Ar–H), 7.47 (2H, m, Ar–H), 7.66 (d, $J = 7.6$ Hz, 2H, Ar–H), 7.77 (1H, brs, Ar–H), 8.10 (1H, s, Ar–H), 12.40 (1H, brs); $^{13}$C-NMR (DMSO-$d_6$, 125 MHz): $\delta = 15.1$ ($CH_3$), 101.3, 111.5, 114.1, 115.5, 118.9, 121.2, 125.1, 128.5, 130.2, 135.1, 137.9, 143.8, 146.4 (C=N), 149.5 (C=O), 156.1 (C=O), 168.3; MS (EI,70 Ev): *m/z* (%) 411 $[M]^+$ (100), 412 $[M + 1]^+$ (24); Anal. Calcd for $C_{23}H_{17}N_5O_3$: C, 67.15; H, 4.16; N, 17.02. Found: C, 67.08; H, 4.23; N, 17.22.

**2-(5-(2,5-Dimethylphenoxy)-3-methyl-1-phenyl-1H-pyrazol-4-yl)-1H-benzo[*d*]- imidazole-5-carboxylic acid (39)** White solid; 37% yield; mp 153–155 °C; IR (KBr) $\upsilon_{max}$: 3432 (NH), 3066, 2925, 1689 (C=O), 1595 (C=N), 1498 (C=C) cm$^{-1}$; $^1$H-NMR (DMSO-$d_6$, 500 MHz): $\delta = 1.96$ (3H, s, $CH_3$), 2.34 (3H, s, $CH_3$), 2.61 (3H, s, $CH_3$), 6.29 (1H, s, Ar–H), 6.63 (d, $J = 8.5$ Hz, 1H, Ar–H), 6.99 (d, $J = 8.0$ Hz, 1H, Ar–H), 7.32 (2H, m, Ar–H), 7.44 (2H, m, Ar–H),7.58 (2H, m, Ar–H), 7.78 (d, $J = 9.5$ Hz, 1H, Ar–H), 8.13 (1H, m, Ar–H); $^{13}$C-NMR (DMSO-$d_6$, 125 MHz): $\delta = 13.6$ ($CH_3$), 16.7 ($CH_3$), 22.1 ($CH_3$), 102.4, 104.6, 106.7, 110.9, 115.1, 122.5, 123.6, 130.1, 130.1, 132.0, 132.3, 137.3, 148.1 (C=N), 154.6 (C–O), 168.8 (C=O); MS (EI,70 Ev): *m/z* (%) 439.2 $[M + 1]^+$ (100), 440.2 $[M + 2]^+$ (25); Anal. Calcd for $C_{26}H_{22}N_4O_3$: C, 71.22; H, 5.06; N, 12.78. Found: C, 71.39; H, 5.21; N, 12.66.

**5-Methyl-2-(3-methyl-5-morpholino-1-phenyl-1H-pyrazol-4-yl)-1H-benzo[*d*]-imidazole (40)** Buff solid; 85% yield; mp: 129–132 °C; IR (KBr) $\upsilon_{max}$: 3423 (NH), 3068, 2960, 1629 (C=N), 1594 (C=C) cm$^{-1}$; $^1$H-NMR (DMSO-$d_6$, 500 MHz): $\delta = 2.24$ (3H, s, $CH_3$), 2.42 (3H, s, $CH_3$), 2.89 (4H, s, H-3, H-5 morpholine protons), 3.48 (4H, s, H-2, H-6 morpholine protons), 7.02 (d, $J = 8.0$ Hz, 1H, Ar–H), 7.39 (2H, m, Ar–H), 7.51 (3H, m, Ar–H), 7.73 (d, $J = 7.5$ Hz, 2H, Ar–H), 12.23 (1H, brs, NH); $^{13}$C-NMR (DMSO-$d_6$, 125 MHz): $\delta = 13.2$ ($CH_3$), 21.4 ($CH_3$), 50.0 (CH-3, CH-5 of morpholine carbons), 66.0 (CH-2, CH-6 of morpholine carbons), 104.5, 124.0, 125.3, 127.2, 129.0, 139.2, 145.5 (C–N), 147.7 (C=N), 148.6 (C–O); MS (EI,70 Ev): *m/z* (%) 374.2 $[M + 1]^+$ (100), 375.2 $[M + 2]^+$ (25); Anal. Calcd for $C_{22}H_{23}N_5O$: C, 70.76; H, 6.21; N, 18.75. Found: C, 70.89; H, 6.35; N, 18.92.

**5-Methyl-2-(3-methyl-1-phenyl-5-(piperidin-1-yl)-1H-pyrazol-4-yl)-1H-benzo[*d*]-imidazole (41)** Buff solid; 80% yield; mp: 116–118 °C; IR (KBr) $\upsilon_{max}$: 3440 (NH), 3068, 2933, 1629 (C=N), 1594 (C=C) cm$^{-1}$; $^1$H-NMR (DMSO-$d_6$, 500 MHz): $\delta = 1.36$ (6H, brs, H-3, H-4, H-5 piperidine protons), 2.19 (3H, s, $CH_3$), 2.42 (3H, s, $CH_3$), 2.82–2.83 (4H, m, H-2, H-6 piperidine protons), 7.02 (d, $J = 8.0$ Hz, 1H, Ar–H), 7.37 (2H, m, Ar–H), 7.46 (d, $J = 8.0$ Hz, 1H, Ar–H), 7.37 (2H, m, Ar–H), 7.71 (d, $J = 7.5$ Hz, 2H, Ar–H); $^{13}$C-NMR (DMSO-$d_6$, 125 MHz): $\delta = 13.1$ ($CH_3$), 21.3 ($CH_3$), 23.3, (CH-4 of piperidine carbons), 25.2, (CH-3, CH-5 of piperidine carbons), 51.0 (CH-2, CH-6 of piperidine carbons), 103.3, 123.1, 123.6, 127.0, 128.9, 130.8, 139.5, 145.6 (C–N), 147.4 (C=N), 149.9 (C–N); MS (EI,70 Ev): *m/z* (%) 372.2 $[M + 1]^+$ (100); Anal. Calcd for $C_{23}H_{25}N_5$: C, 74.36; H, 6.78; N, 18.85. Found: C, 74.20; H, 6.63; N, 18.69.

**5-Methyl-2-(3-methyl-5-(4-methylpiperazin-1-yl)-1-phenyl-1H-pyrazol-4-yl)-1H-benzo[*d*]imidazole (42)** Pale yellow solid; 40% yield; mp:103–104 °C; $^1$H-NMR (DMSO-$d_6$, 400 MHz): $\delta = 2.28$ (3H, s, $CH_3$), 2.44 (3H, s, $CH_3$), 2.71 (3H, s, $CH_3$), 3.05 (4H, brs, piperazine protons), 3.17 (4H, brs, piperazine protons), 7.04 (d, $J = 7.9$ Hz, 1H, Ar–H), 7.43 (2H, m, Ar–H), 7.52 (2H, m, Ar–H), 7.71 (d, $J = 7.7$ Hz, 2H, Ar–H), 12.19 (1H, brs, NH); $^{13}$C-NMR (DMSO-$d_6$, 125 MHz): $\delta = 13.7$ ($CH_3$), 21.8 ($CH_3$), 43.1 (N–$CH_3$), 47.5 (CH-3 + CH-5 piperazine carbons), 53.2 (CH-2 + CH-6 piperazine carbons), 105.2, 123.7, 124.5, 125.7, 127.9, 129.7, 131.4, 139.4, 145.5(C–N), 147.8 (C=N), 147.9 (C=N); Anal. Calcd for $C_{23}H_{26}N_6$: C, 71.48; H, 6.78; N, 21.74. Found: C, 71.59; H, 6.90; N, 21.89.

**5-Methyl-2-(3-methyl-1-phenyl-5-(pyrrolidin-1-yl)-1H-pyrazol-4-yl)-1H-benzo-[*d*]imidazole (43)** Buff solid; 85% yield; mp: 133–135 °C; IR (KBr) $\upsilon_{max}$: 3424 (NH), 3069, 2965, 1630 (C=N), 1593 (C=C) $cm^{-1}$; $^1$H-NMR (DMSO-$d_6$, 500 MHz): $\delta = 1.68$ (4H, brs, H-3, H-4 pyrrolidine protons), 2.19 (3H, s, $CH_3$), 2.41 (3H, s, $CH_3$), 2.93 (4H, brs, H-2, H-5 pyrrolidine protons), 6.99 (d, $J = 7.5$ Hz, 1H, Ar–H), 7.36 (2H, m, Ar–H), 7.44 (d, $J = 8.0$ Hz, 1H, Ar–H), 7.50 (2H, m, Ar–H), 7.58 (d, $J = 7.0$ Hz, 2H, Ar–H); $^{13}$C-NMR (DMSO-$d_6$, 125 MHz): $\delta = 13.2$ ($CH_3$), 21.3 ($CH_3$), 25.0 (CH-3, CH-4 of pyrrolidine carbons), 50.4, (CH-2, CH-5 of pyrrolidine carbons), 101.1, 122.9, 124.1, 127.1, 129.0, 130.7, 140.0, 145.1 (C–N), 147.7 (C=N), 147.7 (C=N); MS (EI,70 Ev): *m/z* (%) 358.2 $[M + 1]^+$ (100), 359.2 $[M + 2]^+$ (25); Anal. Calcd for $C_{22}H_{23}N_5$: C, 73.92; H, 6.49; N, 19.59. Found C, 73.74; H, 6.32; N, 19.39.

**5-Methyl-2-(3-methyl-5-phenoxy-1-phenyl-1H-pyrazol-4-yl)-1H-benzo[*d*]-imidazole (44)** Pale buff solid; 85% yield; mp: 128–130 °C; IR (KBr): $\upsilon_{max}$: 3437 (NH), 3066, 2924, 1627 (C=N), 1595 (C=C) $cm^{-1}$; $^1$H-NMR (DMSO-$d_6$, 500 MHz): $\delta = 2.37$ (3H, s, $CH_3$), 2.61 (3H, s, $CH_3$), 6.94 (4H, m, Ar–H), 7.20 (2H, m, Ar–H), 7.32 (2H, m, Ar–H), 7.40 (d, $J = 8.0$ Hz, 1H, Ar–H), 7.45 (2H, m, Ar–H), 7.66 (d, $J = 8.0$ Hz, 2H, Ar–H); $^{13}$C-NMR (DMSO-$d_6$, 125 MHz): $\delta = 14.9$ ($CH_3$), 21.8 ($CH_3$), 101.6, 115.8, 122.9, 124.4, 124.6, 128.5, 130.2, 130.7, 132.4, 137.6, 144.1 (C–N), 147.1 (C=N), 149.1 (C=N), 156.4 (C–O); MS (EI,70 Ev): *m/z* (%) 381.2, $[M + 1]^+$ (100), 382.2 $[M + 2]^+$ (26); Anal. Calcd for $C_{24}H_{20}N_4O$: C, 75.77; H, 5.30; N, 14.73. Found: C, 75.64; H, 5.41; N, 14.82.

**5-Methyl-2-(3-methyl-1-phenyl-5-(pyridin-2-yloxy)-1H-pyrazol-4-yl)-1H-benzo- [*d*]imidazole (45)** Buff solid; 66% yield; mp: 88–90 °C; IR (KBr) $\upsilon_{max}$: 3424 (NH), 3069, 2925, 1630 (C=N), 1589 (C=C) $cm^{-1}$; $^1$H-NMR (DMSO-$d_6$, 500 MHz): $\delta = 2.37$ (3H, s, $CH_3$), 2.60 (3H, s, $CH_3$), 6.94 (3H, m, Ar–H), 7.21 (2H, m, Ar–H), 7.28 (1H, brs, Ar–H), 7.32 (1H, m, Ar–H), 7.38 (d, 1H, $J = 8.0$ Hz, Ar–H), 7.46 (m, 2H, Ar–H), 7.65 (d, 2H, $J = 7.5$ Hz, Ar–H), 12.06 (brs, 1H, NH); $^{13}$C-NMR (DMSO-$d_6$, 125 MHz): $\delta = 14.6$ ($CH_3$), 21.3 ($CH_3$), 101.5, 115.4, 122.1, 123.2, 123.7, 127.4, 129.4, 129.9, 137.1, 143.6 (C–N), 146.0 (C=N), 148.1 (C=N), 155.8 (C–O); (EI,70 Ev): *m/z* (%) 381.1 $[M]^+$ (100), 382.2 $[M + 1]^+$ (25); Anal. Calcd for $C_{23}H_{19}N_5O$: C, 72.42; H, 5.02; N, 18.36. Found: C, 72.58; H, 5.21; N, 18.49.

**Dimethylphenoxy)-3-methyl-1-phenyl-1H-pyrazol-4-yl)-5-methyl-1H-benzo[*d*]- imidazole (46)** Pale yellow solid; 78% yield; mp: 123–125 °C; IR (KBr) $\upsilon_{max}$: 3424 (NH), 3069, 2925, 1630 (C=N), 1589 (C=C) $cm^{-1}$; $^1$H-NMR (DMSO-$d_6$, 500 MHz): $\delta = 1.98$ (3H, s, $CH_3$), 2.34 (3H, s, $CH_3$), 2.38 (3H, s, $CH_3$), 2.58 (3H, s, $CH_3$), 6.27 (1H, s, Ar–H), 6.64 (d, $J = 9.0$ Hz, 1H, Ar–H), 6.97 (2H, m, Ar–H), 7.32 (2H, m, Ar–H), 7.42 (4H, m, Ar–H), 7.61(2H, m, Ar–H), 11.82 (1H, brs, NH); $^{13}$C-NMR (DMSO-$d_6$,125 MHz): $\delta = 14.5$ ($CH_3$), 15.6 ($CH_3$), 20.5 ($CH_3$), 101.6, 113.3, 122.3, 123.2, 124.0, 127.5, 129.2, 129.2, 131.1, 136.4, 137.2, 146.4 (C–N), 147.9 (C=N), 154.1 (C–O); MS (EI,70 Ev): *m/z* (%) 409.2 $[M + 1]^+$ (100), 410.2 $[M + 2]^+$ (25); Anal. Calcd for $C_{26}H_{24}N_4O$: C, 76.45; H, 5.92; N, 13.72. Found: C, 76.59; H, 5.85; N, 13.64.

**2-(3-Methyl-5-morpholino-1-phenyl-1H-pyrazol-4-yl)-5-nitro-1H-benzo[*d*]-imidazole (47)** Yellow solid; 55% yield; mp: 94–96 °C; IR (KBr) $\upsilon_{max}$: 3424 (NH), 3069, 2925, 1630 (C=N), 1589 (C=C), 1430, 1544 ($NO_2$) $cm^{-1}$; $^1$H-NMR (DMSO-$d_6$, 500 MHz): $\delta = 2.31$ (3H, s, $CH_3$), 2.95 (4H, m, H-3, H-5 morpholine protons), 3.51 (4H, m, H-2, H-6 morpholine protons), 7.42 (1H, m, Ar–H), 7.53 (4H, m, Ar–H), 7.72 (3H, m, Ar–H); MS (EI,70 Ev): *m/z* (%) 405.13 $[M + 1]^+$ (100); Anal. Calcd for $C_{21}H_{20}N_6O_3$: C, 62.37; H, 4.98; N, 20.78. Found: C, 62.29; H, 5.21; N, 20.87.

**2-(3-Methyl-1-phenyl-5-(piperidin-1-yl)-1H-pyrazol-4-yl)-5-nitro-1H-benzo[*d*]-imidazole (48)** Yellow solid; 46% yield; mp: 103–105 °C; IR (KBr) $\upsilon_{max}$: 3424 (NH), 3069, 2925, 1630 (C=N), 1589 (C=C), 1436, 1546 ($NO_2$) $cm^{-1}$; $^1$H-NMR (DMSO-$d_6$, 500 MHz): $\delta = 1.39$ (6H, brs, H-3, H-4, H-5 piperidine protons), 2.27 (3H, s, $CH_3$), 2.87 (4H, brs, H-2, H-6 piperidine protons), 7.54 (6H, m, Ar–H), 8.12 (1H, s, Ar–H), 8.49 (1H, s, Ar–H), 12.87 (1H, brs, NH); $^{13}$C-NMR (DMSO-$d_6$, 125 MHz): $\delta = 14.00$ ($CH_3$), 23.6 (CH-4 piperidine carbons), 25.9 (CH-3, CH-5 of piperidine carbons), 51.5, (CH-2, CH-6 of piperidine carbons), 103.1, 108.8, 112.4, 114.7, 118.4, 122.4, 124.1, 124.6, 128.0, 128.9, 140.0, 143.4 (C–N), 148.0 (C=N), 151.3 (C–$NO_2$); MS (EI,70 Ev): *m/z* (%) 403.2 $[M + 1]^+$ (100), 404.2 $[M + 2]^+$ (25); Anal. Calcd for $C_{22}H_{22}N_6O_2$: C, 65.66; H, 5.51; N, 20.88. Found: C, 65.50; H, 5.43; N, 20.67.

## Biological evaluation

### Molecular docking

The crystal structures of SphK1 in complex with its co-crystalized native ligand: PF-543, as a potent and selective inhibitor of SphK1, the PDB structure of SphK1 (PDB ID: 4V24) was retrieved from the Protein Data Bank, http://www.rcsb.org/pdb/home/home.do. The key amino acids of the active site were identified using data in PDB sum, http://www.ebi.ac.uk/pdbsum/.

Molecular-docking studies of the newly synthesized compounds with SphK1 were performed to gain insight into

the predicted binding affinity and interaction patterns. The 2D and 3D structures of the synthesized compounds were generated using the Chem Draw Ultra v12.0. AutoDock Tools [67] were used for the preparation of docking files supported by AutoDock Vina [67]. In this study, we have performed site-specific molecular docking. The docking was done within 15-Å diameters from the reference PF-543 ligand. The binding site of the crystal structure of SphK1 is composed of the following amino acids: Leu167, Ser168, Ala170, Phe173, Ile174, Val177, Asp178, Phe192, Thr196, Leu259, Leu261, Leu268, Ala274, Phe288, Val290, Leu302, Phe303, Met306, His311, and Ala339. The binding site was defined by including all residues constituting the binding pocket of reference PF-543 ligand.

AutoDock Vina was used for running molecular docking. The docked poses of the newly synthesized compounds with SphK1 were ranked based on the predicted binding affinity and interaction patterns. Intermolecular interactions were studied using PyMol molecular [68]. The 2D plots for protein–ligand interaction were created using the Discovery Studio Visualizer. The top-ranked compounds selected from the analysis are listed in Table 2.

### Expression and purification of SphK1

The secondary cultures of SphK1 were induced by 1-mM IPTG for 4 h followed by centrifugation at 7000 rpm for 15 min to get the cell pellet, which was later resuspended in the lysis buffer and inclusion bodies were prepared as described [56]. Finally, inclusion bodies were solubilized in the solubilization buffer (pH 8.0) comprising 0.5% sarcosine, 50-mM Tris, and 150-mM NaCl. SphK1 was purified using Ni-NTA affinity chromatography, followed by dialysis for 24 h to get the refolded native protein. The purified protein was loaded on SDS-PAGE and the concentration was calculated using a molar absorption coefficient of 48275 $M^{-1}cm^{-1}$ at 280 nm on the Jasco V-660 UV-visible spectrophotometer.

### Fluorescence binding studies

The Jasco Spectrofluorometer at 25 °C was used for the binding studies of all the synthesized compounds. The compounds were first dissolved in DMSO to get the 20-mM stock solution and then diluted to a working concentration of 1 mM in 20-mM Tris and 100-mM NaCl buffer (pH 8.0). The quenching studies were performed with a fixed concentration of SphK1 (5 µM) and the compounds were added gradually in increasing concentration from the 1-mM stocks into the protein solution until the achievement of saturation point. The emission spectra were recorded from 300–400 nm with excitation of SphK1 at 280 nm. The blank titrations (buffer with selected compounds) were subtracted to obtain the final spectra and the quenching data were corrected for the inner filter effect according to the formula, $F = F_{obs}\text{antilog}\ [(A_{ex} + A_{em})/2]$, where $A_{ex}$ and $A_{em}$ is the absorbance of the selected compound at the excitation and emission wavelength, respectively [69]. The quenching spectra obtained for selected compounds were plotted and the inverse correlation between the gradual decrease in the fluorescence intensity with increasing concentration of compounds was used for determining the kinetic parameters ($K_a$ and $n$) from a modified Stern–Volmer equation (Eq. (1) as described [70] where $F_o$ denotes fluorescence intensity of SphK1 without the compound and $F$ denotes the fluorescence intensity of SphK1 at a specific concentration of compound at $\lambda_{max}$.

$$\log \frac{(Fo - F)}{F} = \log Ka + n \log [\text{Ligand}] \quad (1)$$

## Enzyme inhibition assay

A standard Malachite Green (BIOMOL® GREEN reagent) microtitre-plate assay was performed to evaluate the inhibitory potential of all the synthesized compounds against SphK1. Briefly, compounds were incubated with SphK1 (2 µM) for 1 h at 25 °C and then later freshly prepared ATP (200 µM) and 10-mM $MgCl_2$ were added to the protein–ligand mixture. The reaction was allowed to proceed for 30 min at 25 °C. After the required incubation period, the reaction was ended by adding the double amount of BIOMOL® reagent. Finally, a green-colored complex was formed in 10 min and the absorbance readings were recorded on ELISA reader at 620 nm. The reaction with ligands and no protein was also performed to subtract the background reading of inorganic phosphate. A standard phosphate curve was used to determine the loss in activity of SphK1 in terms of amount of phosphate released on treatment with increasing concentrations of selected compounds. The inhibition in SphK1 activity was plotted for selected compounds in terms of percentage as described [56].

**Acknowledgements** This study was supported by the research grant offered by the National Research Centre, Cairo, Egypt, through the internal Project No. 12060119. In addition, this work was supported by the Indian Council of Medical Research through the project No. (BIC/12(01)/2015). We thank the National Cancer Institute (NCI), NIH, Bethesda, Maryland, USA for the performance of the antitumor activity screening through the Developmental Therapeutics Program (DTP). Turab Naqvi is thankful to Indian Council of Medical Research, New Delhi for financial assistance (Project: 45/40/2019-BIO/BMS)".

## Compliance with ethical standards

**Conflict of interest** The authors declare no competing interests.

## References


1. Antoon JW, Beckman BS. Sphingosine kinase: a promising cancer therapeutic target. Cancer Biol Ther. 2011;11:647–50. https://doi.org/10.4161/cbt.11.7.14921.
2. Pyne NJ, El Buri A, Adams DR, Pyne S. Sphingosine 1-phosphate and cancer. Adv Biol Regul. 2018;68:97–106. https://doi.org/10.1016/j.jbior.2017.09.006.
3. Pyne S, Pyne NJ. New perspectives on the role of sphingosine 1-phosphate in cancer. In: Gulbins E, Petrache I, editors. Sphingolipids in disease, Handbook of experimental pharmacology. Vienna: Springer-Verlag; 2013. p. 55–71. https://doi.org/10.1007/978-3-7091-1511-4_3.
4. Schwalm S, Pfeilschifter J, Huwiler A. Sphingosine-1-phosphate: a Janus-faced mediator of fibrotic diseases. BBA-Mol Cell Biol Lipids. 2013;1831:239–50. https://doi.org/10.1016/j.bbalip.2012.07.022.
5. Prager B, Spampinato SF, Ransohoff RM. Sphingosine 1-phosphate signaling at the blood–brain barrier. Trends Mol Med. 2015;21:354–63. https://doi.org/10.1016/j.molmed.2015.03.006.
6. Proia RL, Hla T. Emerging biology of sphingosine-1-phosphate: its role in pathogenesis and therapy. J Clin Invest. 2015;125:1379–87. https://doi.org/10.1172/JCI76369.
7. Reid SP, Tritsch SR, Kota K, Chiang CY, Dong L, Kenny T, et al. Sphingosine kinase 2 is a chikungunya virus host factor co-localized with the viral replication complex. Emerg Microbes Infect. 2015;4:1–9. https://doi.org/10.1038/emi.2015.61.
8. Patwardhan GA, Beverly LJ, Siskind LJ. Sphingolipids and mitochondrial apoptosis. J Bioenerg Biomembr. 2016;48:153–68. https://doi.org/10.1007/s10863-015-9602-3.
9. Ponnusamy S, Meyers-Needham M, Senkal CE, Saddoughi SA, Sentelle D, Selvam SP, et al. Sphingolipids and cancer: ceramide and sphingosine-1-phosphate in the regulation of cell death and drug resistance. Future Oncol. 2010;6:1603–24. https://doi.org/10.2217/fon.10.116.
10. Berwick ML, Dudley BA, Maus K, Chalfant CE. The role of ceramide 1-phosphate in inflammation, cellular proliferation, and wound healing. Adv Exp Med Biol. 2019;1159:65–77. https://doi.org/10.1007/978-3-030-21162-2_5.
11. Tsai HC, Han MH. Sphingosine-1-phosphate (S1P) and S1P signaling pathway: therapeutic targets in autoimmunity and inflammation. Drugs. 2016;76:1067–79. https://doi.org/10.1007/s40265-016-0603-2.
12. Hatoum D, Haddadi N, Lin Y, Nassif NT, McGowan EM. Mammalian sphingosine kinase (SphK) isoenzymes and isoform expression: challenges for SphK as an oncotarget. Oncotarget. 2017;8:36898. 10.18632%2Foncotarget.16370.
13. Melendez AJ, Carlos-Dias E, Gosink M, Allen JM, Takacs L. Human sphingosine kinase: molecular cloning, functional characterization and tissue distribution. Gene. 2000;251:19–26. https://doi.org/10.1016/S0378-1119(00)00205-5.
14. Gault CR, Obeid LM, Hannun YA. An overview of sphingolipid metabolism: from synthesis to breakdown. Adv Exp Med Biol. 2010;688:1–23. https://doi.org/10.1007/978-1-4419-6741-1_1.
15. Shida D, Takabe K, Kapitonov D, Milstien S, Spiegel S. Targeting SphK1 as a new strategy against cancer. Curr Drug Targets. 2008;9:662–73. https://doi.org/10.2174/138945008785132402.
16. Aoyagi T, Nagahashi M, Yamada A, Takabe K. The role of sphingosine-1-phosphate in breast cancer tumor-induced lymphangiogenesis. Lymphat Res Biol. 2012;10:97–106. https://doi.org/10.1089/lrb.2012.0010.
17. Nagahashi M, Yamada A, Katsuta E, Aoyagi T, Huang WC, Terracina KP, et al. Targeting the SphK1/S1P/S1PR1 axis that links obesity, chronic inflammation, and breast cancer metastasis. Cancer Res. 2018;78:1713–25. https://doi.org/10.1158/0008-5472.CAN-17-1423.
18. Wang F, Wu Z. Sphingosine kinase 1 overexpression is associated with poor prognosis and oxaliplatin resistance in hepatocellular carcinoma. Exp Ther Med. 2018;15:5371–6. https://doi.org/10.3892/etm.2018.6086.
19. Aoki H, Aoki M, Katsuta E, Ramanathan R, Idowu MO, Spiegel S, et al. Host sphingosine kinase 1 worsens pancreatic cancer peritoneal carcinomatosis. J Surg Res. 2016;205:510–7. https://doi.org/10.1016/j.jss.2016.05.034.
20. Furuya H, Shimizu Y, Tamashiro PM, Iino K, Bielawski J, Chan OT, et al. Sphingosine kinase 1 expression enhances colon tumor growth. J Transl Med. 2017;15:1–8. https://doi.org/10.1186/s12967-017-1220-x.
21. Ogretmen B, Hannun YA. Biologically active sphingolipids in cancer pathogenesis and treatment. Nat Rev Cancer. 2004;4:604–16. https://doi.org/10.1038/nrc1411.
22. Clemens JJ, Davis MD, Lynch KR, Macdonald TL. Synthesis of para-alkyl aryl amide analogues of sphingosine-1-phosphate: discovery of potent S1P receptor agonists. Bioorg Med Chem Lett. 2003;13:3401–4. https://doi.org/10.1016/S0960-894X(03)00812-6.
23. Igarashi Y, Hakomori S, Toyokuni T, Dean B, Fujita S, Sugimoto M, et al. Effect of chemically well-defined sphingosine and its N-methyl derivatives on protein kinase C and src kinase activities. Biochemistry. 1989;28:6796–800. https://doi.org/10.1021/bi00443a002.
24. Plano D, Amin S, Sharma AK. Importance of sphingosine kinase (SphK) as a target in developing cancer therapeutics and recent developments in the synthesis of novel SphK inhibitors: miniperspective. J Med Chem. 2014;57:5509–24. https://doi.org/10.1021/jm4011687.
25. Paugh SW, Paugh BS, Rahmani M, Kapitonov D, Almenara JA, Kordula T, et al. A selective sphingosine kinase 1 inhibitor integrates multiple molecular therapeutic targets in human leukemia. Blood. 2008;112:1382–91. https://doi.org/10.1182/blood-2008-02-138958.
26. Kappos L, Radue EW, O'Connor P, Polman C, Hohlfeld R, Calabresi P, et al. A placebo-controlled trial of oral fingolimod in relapsing multiple sclerosis. N Engl J Med. 2010;362:387–401. https://doi.org/10.1056/NEJMoa0909494.
27. Schnute ME, McReynolds MD, Kasten T, Yates M, Jerome G, Rains JW, et al. Modulation of cellular S1P levels with a novel, potent and specific inhibitor of sphingosine kinase-1. Biochem J. 2012;444:79–88. https://doi.org/10.1042/BJ20111929.
28. Schnute ME, McReynolds MD, Carroll J, Chrencik J, Highkin MK, Iyanar K, et al. Discovery of a potent and selective sphingosine kinase 1 inhibitor through the molecular combination of chemotype-distinct screening hits. J Med Chem. 2017;60:2562–72. https://doi.org/10.1021/acs.jmedchem.7b00070.
29. French KJ, Schrecengost RS, Lee BD, Zhuang Y, Smith SN, Eberly JL, et al. Discovery and evaluation of inhibitors of human sphingosine kinase. Cancer Res. 2003;63:5962–9.
30. Gao P, Peterson YK, Smith RA, Smith CD. Characterization of isoenzyme-selective inhibitors of human sphingosine kinases. PloS ONE. 2012;7:e44543. https://doi.org/10.1371/journal.pone.0044543.
31. Gandy KAO, Obeid LM. Targeting the sphingosine kinase/sphingosine 1-phosphate pathway in disease: review of sphingosine kinase inhibitors. BBA-Mol Cell Biol Lipids. 2013;1831:157–66. https://doi.org/10.1016/j.bbalip.2012.07.002.
32. Wang J, Knapp S, Pyne NJ, Pyne S, Elkins JM. Crystal structure of sphingosine kinase 1 with PF-543. ACS Med Chem Lett. 2014;5:1329–33. https://doi.org/10.1021/ml5004074.
33. Gustin DJ, Li Y, Brown ML, Min X, Schmitt MJ, Wanska M, et al. Structure guided design of a series of sphingosine kinase

(SphK) inhibitors. Bioorg Med Chem Lett. 2013;23:4608–16. https://doi.org/10.1016/j.bmcl.2013.06.030.
34. Hengst JA, Wang X, Sk UH, Sharma AK, Amin S, Yun JK. Development of a sphingosine kinase 1 specific small-molecule inhibitor. Bioorg Med Chem Lett. 2010;20:7498–502. https://doi.org/10.1016/j.bmcl.2010.10.005.
35. Singla P, Luxami V, Paul K. Benzimidazole-biologically attractive scaffold for protein kinase inhibitors. RSC Adv. 2014;4:12422–40. https://doi.org/10.1039/C3RA46304D.
36. Edward HJ, Vibha O, Ammar A, Kate B, Lillian C, Gurmit G, et al. Identification and optimization of benzimidazole sulfonamides as orally bioavailable sphingosine 1-phosphate receptor 1 antagonists with in vivo activity. J Med Chem. 2015;8:7057–75. https://doi.org/10.1021/acs.jmedchem.5b01078.
37. Garuti L, Roberti M, Bottegoni G. Benzimidazole derivatives as kinase inhibitors. Curr Med Chem. 2014;21:2284–98. https://doi.org/10.2174/0929867321666140217105714.
38. Akhtar W, Khan MF, Verma G, Shaquiquzzaman M, Rizvi M, Mehdi SH, et al. Therapeutic evolution of benzimidazole derivatives in the last quinquennial period. Eur J Med Chem. 2017;126:705–53. https://doi.org/10.1016/j.ejmech.2016.12.010.
39. Akhtar MJ, Siddiqui AA, Khan AA, Ali Z, Dewangan RP, Pasha S, et al. Design, synthesis, docking and QSAR study of substituted benzimidazole linked oxadiazole as cytotoxic agents, EGFR and erbB2 receptor inhibitors. Eur J Med Chem. 2017;126:853–69. https://doi.org/10.1016/j.ejmech.2016.12.014.
40. Galal SA, Khattab M, Shouman SA, Ramadan R, Kandil OM, Tabll A, et al. Novel checkpoint kinase 2 (Chk2) inhibitors; design, synthesis and biological evaluation of pyrimidine-benzimidazole conjugates. Eur J Med Chem. 2018;146:687–708. https://doi.org/10.1016/j.ejmech.2018.01.072.
41. Galal SA, Khairat SH, Ali HI, Shouman SA, Attia YM, Ali MM, et al. New candidates of pyrazole-benzimidazole conjugates as checkpoint kinase 2 (Chk2) inhibitors. Eur J Med Chem. 2018;144:859–73. https://doi.org/10.1016/j.ejmech.2017.12.023.
42. Galal SA, Abdelsamie AS, Shouman SA, Attia YM, Ali HI, Tabll A, et al. Design, synthesis and biological evaluation of novel pyrazole-benzimidazole conjugates as checkpoint kinase 2 (Chk2) inhibitors with studying their activities alone and in combination with genotoxic drugs. Eur J Med Chem. 2017;134:392–405. https://doi.org/10.1016/j.ejmech.2017.03.090.
43. Abdullaziz MA, Abdel-Mohsen HT, El Kerdawy AM, Ragab FA, Ali MM, Abu-bakr SM, et al. Design, synthesis, molecular docking and cytotoxic evaluation of novel 2-furybenzimidazoles as VEGFR-2 inhibitors. Eur J Med Chem. 2017;136:315–29. https://doi.org/10.1016/j.ejmech.2017.04.068.
44. Flanagan KJ, Shaker YM, Temirak A, El Diwani HI. Crystal structures of 2-furylbenzimidazoles with antiangiogenic inhibition of VEGF in cell line MCF-7. Heterocycles. 2015;91:1603–13. https://doi.org/10.3987/COM-15-13258.
45. Shaker YM, Omar MA, Mahmoud K, Elhallouty SM, El-Senousy WM, Ali MM, et al. Synthesis, in vitro and in vivo antitumor and antiviral activity of novel 1-substituted benzimidazole derivatives. J Enzym Inhib Med Chem. 2015;30:826–45. https://doi.org/10.3109/14756366.2014.979344.
46. Temirak A, Shaker YM, Ragab FA, Ali MM, Soliman SM, Mortier J, et al. Synthesis, biological evaluation, and docking studies of new 2-furylbenzimidazoles as anti-angiogenic agents: part II. Arch Pharm. 2014;347:291–304. https://doi.org/10.1002/ardp.201300356.
47. Temirak A, Shaker YM, Ragab FA, Ali MM, Ali HI, El Diwani HI. Part I. Synthesis, biological evaluation and docking studies of new 2-furylbenzimidazoles as antiangiogenic agents. Eur J Med Chem. 2014;87:868–80. https://doi.org/10.1016/j.ejmech.2014.01.063.
48. Galal SA, Khairat SH, Ragab FA, Abdelsamie AS, Ali MM, Soliman SM, et al. Design, synthesis and molecular docking study of novel quinoxalin-2 (1H)-ones as anti-tumor active agents with inhibition of tyrosine kinase receptor and studying their cyclooxygenase-2 activity. Eur J Med Chem. 2014;86:122–32. https://doi.org/10.1016/j.ejmech.2014.08.048.
49. Galal SA, Abdelsamie AS, Soliman SM, Mortier J, Wolber G, Ali MM, et al. Design, synthesis and structure–activity relationship of novel quinoxaline derivatives as cancer chemopreventive agent by inhibition of tyrosine kinase receptor. Eur J Med Chem. 2013;69:115–24. https://doi.org/10.1016/j.ejmech.2013.07.049.
50. Santos WL, Lynch KR. Drugging sphingosine kinases. ACS Chem Biol. 2015;10:225–33. https://doi.org/10.1021/cb5008426.
51. Pitman MR, Costabile M, Pitson SM. Recent advances in the development of sphingosine kinase inhibitors. Cell Signal. 2016;28:1349–63. https://doi.org/10.1016/j.cellsig.2016.06.007.
52. Prajuli R, Banerjee J, Khanal H. Synthesis of some pyrazolone derivatives and evaluation of its antibacterial and cytotoxic activity. Orient J Chem. 2015;31:2099–106. https://doi.org/10.13005/ojc/310430.
53. Dikusar E, Potkin V, Kozlov N. Synthesis of E-3-alkoxy-4-hydroxy (alkoxy, acyloxy)-phenylmethylene (2-hydroxyphenyl) amines. Russ J Gen Chem. 2009;79:258–63. https://doi.org/10.1134/S1070363209020157.
54. Rabong C, Hametner C, Mereiter K, Kartsev V, Jordis U. Scope and limitations of the T-reaction employing some functionalized CH-acids and naturally occurring secondary amines. Heterocycles. 2008;75:799–838. https://doi.org/10.3987/COM-07-11260.
55. Park HJ, Lee K, Park SJ, Ahn B, Lee JC, Cho H, et al. Identification of antitumor activity of pyrazole oxime ethers. Bioorg Med Chem Lett. 2005;15:3307–12. https://doi.org/10.1016/j.bmcl.2005.03.082.
56. Roy S, Mahapatra AD, Mohammad T, Gupta P, Alajmi MF, Hussain A, et al. Design and development of novel urea, sulfonyl triurea, and sulfonamide derivatives as potential inhibitors of sphingosine kinase1. Pharmaceuticals. 2020;13:118–40. https://doi.org/10.3390/ph13060118.
57. Roy S, Mohammad T, Gupta P, Dahiya R, Parveen S, Luqman S, et al. Discovery of harmaline as a potent inhibitor of sphingosine kinase-1: a chemopreventive role in lung cancer. ACS Omega. 2020;5:21550–60. https://doi.org/10.1021/acsomega.0c02165.
58. Hetényi C, van der SD. Blind docking of drug-sized compounds to proteins with up to a thousand residues. FEBS Lett. 2006;580:1447–50. https://doi.org/10.1016/j.febslet.2006.01.074.
59. Gupta P, Khan FI, Roy S, Anwar S, Dahiya R, Alajmi MF, et al. Functional implications of PH induced conformational changes in the sphingosine kinase 1. Spectrochim Acta Part A. 2020;225:117453–64. https://doi.org/10.1016/j.saa.2019.117453.
60. Roy S, Mohammad T, Gupta P, Dahiya R, Parveen S, Luqman S, et al. Discovery of harmaline as a potent inhibitor of sphingosine kinase-1: a chemopreventive role in lung cancer. ACS Omega. 2020;34:21550–60. https://doi.org/10.1021/acsomega.0c02165.
61. Gupta P, Mohammad T, Dahiya R, Roy S, Noman OMA, Alajmi MF, et al. Evaluation of binding and inhibition mechanism of dietary phytochemicals with sphingosine kinase 1: towards targeted anticancer therapy. Sci Rep. 2019;9:1–15. https://doi.org/10.1038/s41598-019-55199-3.
62. Gupta P, Mohammad T, Khan P, Alajmi MF, Hussain A, Rehman MT, et al. Evaluation of ellagic acid as an inhibitor of sphingosine kinase 1: a targeted approach towards anticancer therapy. Biomed Pharmacother. 2019;118:109245–57. https://doi.org/10.1016/j.biopha.2019.109245.
63. Trott O, Olson AJ. AutoDock Vina: improving the speed and accuracy of docking with a new scoring function, efficient optimization, and multithreading. J Comput Chem. 2010;31:455–61. https://doi.org/10.1002/jcc.21334.
64. Zheng X, Li W, Ren L, Liu J, Pang X, Chen X, et al. The sphingosine kinase-1/sphingosine-1-phosphate axis in cancer: Potential target for anticancer therapy. Pharmacol Ther. 2019;195:85–99. https://doi.org/10.1016/j.pharmthera.2018.10.011.

65. Gupta P, Taiyab A, Hussain A, Alajmi MF, Islam A, Hassan M. Targeting the sphingosine kinase/sphingosine-1-phosphate signaling axis in drug discovery for cancer therapy. Cancers. 2021;13:1898. https://doi.org/10.3390/cancers13081898.
66. National Cancer Institute. Developmental therapeutic program. www.dtp.nci.nih.gov.
67. Morris GM, Huey R, Lindstrom W, Sanner MF, Belew RK, Goodsell DS, et al. AutoDock4 and AutoDockTools4: automated docking with selective receptor flexibility. J Comput Chem. 2009;30:2785–91. https://doi.org/10.1002/jcc.21256.
68. Schrodinger LLC. The PyMOL Molecular Graphics System, Version 1.8. 2015.
69. Bakar KA, Feroz SR. A critical view on the analysis of flurosecence quenching data for determining ligand-protein binding affinity. Spectrochim Acta Part A. 2019;223:117337–42. https://doi.org/10.1016/j.saa.2019.117337.
70. Boaz H, Rollefson G. The quenching of fluorescence. Deviations from the Stern-Volmer law. J Am Chem Soc. 1950;72:3435–43. https://doi.org/10.1021/ja01164a032.